Thermodynamics and Lattice Vibrations of Minerals: 3. Lattice Dynamics and an Approximation for Minerals With Application to Simple Substances and Framework Silicates

SUSAN WERNER KIEFFER[1]

Department of Earth and Space Sciences, University of California, Los Angeles, California 90024

The principles of lattice dynamics are briefly reviewed in this paper, and from these principles a simple, generally applicable lattice vibrational spectrum is proposed for minerals. The spectrum can be used to calculate the thermodynamic functions in the harmonic approximation. The model proposed is consistent with lattice dynamics and is sufficiently detailed in its assumptions about the distribution of modes that the thermodynamic functions are closely specified. The primitive unit cell, containing s atoms, is chosen as the fundamental vibrating unit; it has $3s$ degrees of freedom, three of which are acoustic modes. Anisotropy of these modes is included by use of anisotropic shear velocities for the two shear branches: dispersion is included by use of a sinusoidal dispersion relation between frequency and wave vector for all three acoustic branches. Optic modes, which comprise $3s - 3$ degrees of freedom, are represented by a uniform continuum, except for 'intramolecular' stretching modes (such as Si-O stretching modes) which can be enumerated and identified as being isolated from the optic continuum. Parameters for the model are obtained from elastic and spectroscopic data; the model is independent of any calorimetric data. It is applied to give the temperature dependence of C_V over the range 0°–1000°K of halite, periclase, brucite, corundum, spinel, quartz, cristobalite, silica glass, coesite, stishovite, rutile, albite, and microcline. The specific heat of the simple Debyelike substances, halite and periclase, is reproduced well by the model. The influence of the additional formula unit of H_2O on the vibrational and thermodynamic properties of brucite, as compared to periclase, is discussed. The heat capacities of the relatively simple minerals, spinel and corundum, are given accurately by the model. The heat capacities of quartz, cristobalite, and coesite are accurately predicted from spectroscopic data through the model. The heat capacity of silica glass is discussed in terms of the classic continuous random network (CRN) model and a paracrystalline model, the pentagonal dodecahedral (PD) model of Robinson (1965). The PD model appears to be more consistent with measured C_V data than the CRN model. The heat capacity data of rutile are reasonably reproduced by the model as are the data for stishovite at temperatures above 50°K. Measured data for stishovite below 50°K appear to contain an excess heat capacity relative to the model; this excess may arise from surface energy contributions, as was suggested by Holm et al. (1967), and it is suggested that the model provides a better estimate of the low-temperature vibrational heat capacity of stishovite than the measured data. The heat capacities of albite and microcline are reproduced well by the model. The model is only a simple approximation to real lattice vibrational spectra, but it appears to work well for a large number of minerals and is therefore useful in correlating structural, compositional, elastic, spectroscopic, and thermodynamic properties for purposes of extrapolation and prediction of these properties.

CONTENTS

1. INTRODUCTION

In the previous two papers of this series [*Kieffer*, 1979*a*, *b*], referred to as paper 1 and paper 2, respectively, the vibrational characteristics of silicates as known from simple one-dimensional theory and from experimental data have been reviewed, and the influence of various effects such as anisotropy, dispersion, and low- and high-frequency optic modes on the heat capacity has been discussed in a general way. In this paper, several principles which can be used to formulate a generally applicable model for the thermodynamic functions of minerals are extracted from lattice dynamics theory. The model proposed lacks the rigor of formal lattice dynamics, but it is generally and easily applicable to a large variety of substances of geologic interest. This approach provides a method for calculating the thermodynamic functions which is independent of any calorimetric data; the only data required are elastic wave velocities, crystallographic parameters, and spectral frequencies. In this paper the model is illustrated with calculations of the temperature dependence of the heat capacity for the 'simple substances' halite, periclase, brucite, corundum, spinel, stishovite, and rutile and the framework silicates quartz, cristobalite, coesite, silica glass, albite, and microcline. The effects of structure and composition on the lattice vibrations and hence on the thermodynamic functions are discussed.

[1] Now at U.S. Geological Survey, Flagstaff, Arizona 86001.

Paper number 8R1055.
0034-6853/79/018R-1055$06.00

2. LATTICE DYNAMICS: SUMMARY OF PRINCIPLES

Vibrating Unit of the Crystal

The theory of lattice dynamics is based on the principle of translational invariance of the lattice as expressed in Bloch's theorem: 'For any wave-function/state function that satisfies the Schrödinger equation (or its classical or quantal equivalent) there exists a vector **K** such that translation by a lattice vector **a** is equivalent to multiplying by the phase factor exp $(i\mathbf{K}\cdot\mathbf{a})$' [*Ziman*, 1972, p. 17]. Therefore in lattice dynamics the fundamental vibrating unit of the lattice is taken as the Bravais or primitive unit cell [e.g., *Born and Huang*, 1954, chapter 5]. If there are s particles in the Bravais cell (where $s = Zn$, Z is the number of formula units in the cell, and n is the number of particles in the formula on which the molecular weight is based), there are $3s$ degrees of freedom associated with the cell and $3sN_A/Z = 3nN_A$ degrees of freedom in one mole of the substance. (Symbols are defined in the notation list.)

The Bravais unit cell of some lattices does not coincide with the more commonly used crystallographic cell. Early investigators in the field of vibrational properties of solids sometimes used a larger unit cell than the Bravais cell as the vibrating unit. For example, *Raman* [1943, 1961] formulated a lattice dynamical theory for sodium chloride in terms of a supercell, the fundamental Bravais cell doubled in length along each dimension. The vibrational modes of such a supercell are enumerated differently from those of a Bravais cell; the difference between the Raman model and current lattice dynamics models will be discussed in section 5.

Modes of Vibration of Crystals

Many formulations of the problem of small-amplitude vibrations of a lattice are possible [e.g., *Born and Huang*, 1954; *Blackman*, 1955; *Maradudin et al.*, 1963; *Wallace*, 1972], but the main results are similar in all cases. The following is a summary of the detailed analysis of *Born and Huang* [1954, chapter 5] and is simply a generalized form of the discussion presented in paper 1 for monatomic and diatomic lattices. The formulation is outlined here to show briefly the argument which leads to a separation of acoustic and optic modes and their enumeration for polyatomic substances.

Consider a perfect crystal lattice. The position vector of a particle may be represented as

$$\mathbf{x}\begin{pmatrix} j \\ r \end{pmatrix} = \mathbf{x}(j) + \mathbf{x}(r)$$

where the position within the unit cell is designated as $\mathbf{x}(r)$ and the distance of the unit cell from the origin is $\mathbf{x}(j)$. In these expressions, j is the cell index ($j = 1, 2, 3, \cdots$), and r is the base index ($r = 1, 2, 3, \cdots$) which distinguishes different nuclei in the cell. The Cartesian components of the instantaneous displacement of a particle of mass m_r from its equilibrium position are denoted as

$$\mu_\alpha\begin{pmatrix} j \\ r \end{pmatrix} \qquad \alpha = 1, 2, 3$$

The potential energy of the structure, in terms of the displacements of the particles, is denoted by Φ. The equations of motion of a particle of mass m_r are

$$m_r\ddot{\mu}_\alpha\begin{pmatrix} j \\ r \end{pmatrix} = -\frac{\partial\Phi}{\partial\mu_\alpha\begin{pmatrix} j \\ r \end{pmatrix}} \tag{1}$$

For small-amplitude vibrations the potential Φ may be expanded as a Taylor series in powers of the atomic displacements to terms of second order, with the result that the derivative on the right side of (1) becomes

$$\frac{\partial\Phi}{\partial\mu_\alpha\begin{pmatrix} j \\ r \end{pmatrix}} = \sum_{j'r'\beta}\Phi_{\alpha\beta}\begin{pmatrix} j\,j' \\ r\,r' \end{pmatrix}\mu_\beta\begin{pmatrix} j' \\ r' \end{pmatrix} \tag{2}$$

Hence the equations of motion for particle m_r become

$$m_r\ddot{\mu}_\alpha\begin{pmatrix} j \\ r \end{pmatrix} = -\sum_{j'r'\beta}\Phi_{\alpha\beta}\begin{pmatrix} j\,j' \\ r\,r' \end{pmatrix}\mu_\beta\begin{pmatrix} j' \\ r' \end{pmatrix} \tag{3}$$

There are an infinite number of these equations of motion (involving a triple summation over all cells j' ($0 < j' < \infty$), over all particles in a unit cell, r' ($0 < r' < s - 1$), and over three directions, β ($\beta = 1, 2, 3$)). Reduction of this infinite number of simultaneous differential equations to a finite number follows from Bloch's theorem that the basic property of lattice periodicity allows wavelike solutions of the form

$$\mu_\alpha\begin{pmatrix} j \\ r \end{pmatrix} = \frac{1}{(m_r)^{1/2}}W_\alpha(r)\exp\left\{i\mathbf{K}\cdot\mathbf{x}\begin{pmatrix} j \\ r \end{pmatrix} - i\omega t\right\} \tag{4}$$

where **K** is an arbitrary wave vector in reciprocal space. The above equation is the generalized form of (18) and (25) in paper 1 for the monatomic and diatomic cases, respectively. In the theory of vibrations of elastic continua, the magnitude of $\mathbf{y} = \mathbf{K}/2\pi$ is proportional to the reciprocal of the wavelength of an elastic wave, and its direction is the direction of the propagating wave. $W_\alpha(r)$ is the wave amplitude and may depend on **K** or on r through a phase function, but it is independent of the cell index j. The angular frequency is ω ($= 2\pi\nu$).

From the assumption of (4) a set of $3s$ linear homogeneous equations in the $3s$ unknowns $W_\alpha(r)$ ($r = 0,1,2,\cdots s - 1$; $\alpha = 1, 2, 3$) is obtained (corresponding to (29*a*) and (29*b*) in paper 1 for the diatomic case):

$$\omega^2 W_\alpha(r) = \sum_{r'\beta} C_{\alpha\beta}\begin{pmatrix} \mathbf{K} \\ rr' \end{pmatrix}W_\beta(r') \tag{5}$$

where the coefficients $C_{\alpha\beta}$ are complicated functions of the lattice potential coefficients (given by *Born and Huang* [1954, p. 224]). The $3s$ equations are soluble if

$$\left|\omega^2\delta_{\alpha\beta}\delta_{rr'} - C_{\alpha\beta}\begin{pmatrix} \mathbf{K} \\ rr' \end{pmatrix}\right| = 0 \tag{6}$$

where $\delta_{\alpha\beta}$ is the Kronecker delta function. The determinant on the left is known as the 'secular determinant' and is a determinant equation of $3s^{\text{th}}$ degree in ω^2. Equation (30) in section 3 in paper 1 is the secular equation for the linear diatomic chain. The $3s$ solutions for each value of **K** are designated as $\omega_i^2(\mathbf{K})$, where $i = 1, 2, \cdots, 3s$. It can be proved that the eigenvalues $\{\omega_i^2(\mathbf{K})\}$ are the squares of the normal mode frequencies of the crystal: $\omega^2(\mathbf{K})$ is a multivalued function of **K** and the $3s$ solutions for each value of **K** can be regarded as 'branches' of the multivalued function $\omega^2(\mathbf{K})$. If the lattice has a high degree of symmetry, these branches may coincide for certain values of **K**. The relations $\omega = \omega_i(\mathbf{K})$ for $1 \le i \le 3s$ are known as the 'dispersion relations.' Dispersion relations for simple monatomic and diatomic substances were discussed in paper 1. For each of the $3s$ values of $\omega_i^2(\mathbf{K})$ corresponding to a given **K**, there exists an eigenvector

$$\mathbf{w}\begin{pmatrix} r \\ i \end{pmatrix}\Big|\mathbf{K}$$

whose components are the solutions to (5).

The matrix of the coefficients $C_{\alpha\beta}$ is known as the dynamical matrix. It is Hermitian, and therefore the eigenvalues $\{\omega_i^2(\mathbf{K})\}$ are real. The microscopic condition for stability of the lattice is that the $\omega_i^2(\mathbf{K})$ be positive. It follows that $\omega_i(\mathbf{K})$ is either real or purely imaginary. If $\omega_i(\mathbf{K})$ were purely imaginary, vibrational motion of the lattice would erupt exponentially into the past or future [*Maradudin et al.*, 1963]. Therefore only real $\omega_i(\mathbf{K})$ represent lattice waves.

Enumeration of acoustic and optic modes follows from examination of limiting values of $\mathbf{K} \to \mathbf{0}$ [*Born and Huang*, 1954, pp. 230–232] (this is the long-wavelength limit at which physical observations are frequently made). In the long-wavelength limit, $\mathbf{K}$ is set equal to zero in the coefficients $C_{\alpha\beta}$ and in (5) for the eigenvector $\mathbf{W}(r)$. As $\mathbf{K} \to \mathbf{0}$, one of the $\omega_i^2(\mathbf{0})$ vanishes for $\alpha = 1, 2, 3$ [*Born and Huang*, 1954, p. 229]. Therefore there are three solutions which vanish with vanishing $\mathbf{K}$. In this limit, all particles in each unit cell move in parallel and with equal amplitudes. This motion is characteristic of elastic deformation under sound waves, and hence these three branches are termed 'acoustic branches.' The remaining $3s - 3$ modes whose frequencies do not vanish at $\mathbf{K} = \mathbf{0}$ are called 'optic modes,' because these modes can interact with photons if the particles bear opposite electrical charges.

In summary, there are three acoustic branches and $3s - 3$ optic branches for each wave vector $\mathbf{K}$. Dispersion relations for polyatomic solids were shown in Figure 5 of paper 2. The exact behavior of the dispersion curves is complicated and it is therefore not possible to specify the shapes of the dispersion relations without further knowledge of the interatomic potential Φ and the coefficients $C_{\alpha\beta}$. However, the useful general result which emerges from lattice dynamics is that all of the roots $\omega_i(\mathbf{K})$ as a function of $\mathbf{K}$ are continuous and have the periodicity of the reciprocal lattice [e.g., *Ziman*, 1972, p. 36].

At this point it should be noted that it is sometimes convenient and instructive to consider the vibrations of structural units other than the Bravais unit cell. For example, if a monatomic linear chain is treated as a diatomic chain (two atoms per unit cell) with a mass ratio approaching 1, a spurious optic mode is generated. This optic mode is actually the acoustic branch folded back into the artificially small Brillouin zone generated by the choice of a supercell. Similarly, a diatomic linear chain may be treated as a monatomic chain which contains new Brillouin zone boundaries across which the frequencies are discontinuous. These classic examples are discussed in many elementary texts; the discussion by *Brillouin* [1953, chapter 4] is particularly good. Such considerations of non-Bravais structural units are consistent with lattice dynamics if the ratio of acoustic to optic modes ($3/3s$) based on the vibrations of a Bravais cell is not altered.

Fortunately, for calculation of the thermodynamic functions an accurate description of the dispersion relations $\omega_i(\mathbf{K})$ is not required, but rather, a description of the lattice vibration spectrum $g(\omega)$, and it will prove sufficient for our purposes to extract the major conclusions of this section for use in the model. Many methods of calculating or estimating $g(\omega)$ have been proposed; the major methods are reviewed in the next section.

Brief Review of Methods of Calculating $g(\omega)$

The previous discussion demonstrates that an accurate calculation of $g(\omega)$ requires (1) the knowledge of interatomic forces among large numbers of atoms, (2) the solution of the equations of motion for a large number of wave vectors, and (3) the integration of the dispersion relations over all of wave vector space. Because little is known regarding the nature of interatomic forces, the practice has been to assume simple models for forces (e.g., bond-bending and bond-stretching forces) and to calculate their magnitudes from the experimental values of elastic constants, optical frequencies at $\mathbf{K} = \mathbf{0}$, and, more recently, inelastic neutron scattering data which give dispersion relations in several directions in crystals. From calculated or measured dispersion curves in high-symmetry directions and calculated curves in other directions in the Brillouin zone in which the normal modes have not been observed, $g(\omega)$ is obtained by numerical integration over the zone volume, a tedious process now eased by the use of high-speed computers. This method was introduced by Blackman and refined by Houston; *Blackman* [1955], *Leibfried* [1955], *Maradudin et al.* [1963], and *Cochran* [1971] provide detailed reviews of numerical methods of calculation of $g(\omega)$.

For a few simple substances, force models which take into account as many as sixth-neighbor interactions have been successful in predicting dispersion laws for crystals and thus the low-temperature behavior of C_V. A sodium chloride spectrum calculated by *Neuberger and Hatcher* [1961] was reproduced as Figure 3 in paper 2 and is used in section 6 for comparison with the proposed model. This spectrum and an earlier NaCl spectrum calculated by *Kellerman* [1940] both yield good agreement with measured heat capacities C_V or calorimetric Debye temperatures $\theta_{cal}(T)$ for NaCl. *Raubenheimer and Gilat* [1967] show that the observed 40% decrease in $\theta_{cal}(T)$ of zinc (hcp) between 0° and 15°K is predictable from a force-constant model. An effect of similar magnitude was calculated for white tin (tetragonal) by *Kam and Gilat* [1968] from a Born–von Karman force model. *Walker* [1956] has shown that a consideration of anharmonic effects is necessary to predict $\theta_{cal}(T)$ accurately for aluminum by fitting the Born model of lattice vibrations to experimental phonon dispersion curves obtained from diffuse scattering of X rays. A good fit to the heat capacity at low temperatures was obtained for sodium by *Dixon et al.* [1963], using phonon dispersion relations obtained by inelastic neutron scattering experiments.

The calculations of these and many other authors have shown that the lattice dynamical theory is essentially correct, being limited mainly by the lack of information on interatomic forces and possibly by considerations of anharmonic effects. The theory is powerful because it correlates thermal, elastic, and dielectric properties with the fundamental interactions among the atoms. In practice, the use of this method involves formidable calculations, and it has been used only for relatively simple crystals.

Another method of interest, but as yet limited application, is the method of moments [*Montroll*, 1942, 1943]. In this approximation the frequency distribution is expanded in terms of moments of the spectrum, the moments being obtained from the trace of the characteristic matrix [*Born and Huang*, 1954, p. 72]. This method has successfully accounted for thermodynamic properties of some cubic substances.

Many authors have attempted to find a simpler representation of $g(\omega)$ than that given by the lattice dynamical theory by using combinations of Einstein and Debye terms. One of the earliest approximations was that of Nernst and Lindemann in 1911 [see *Blackman*, 1955], who proposed a combination of two Einstein oscillators to represent the specific heat according to

$$C_V = (3Nk/2)\,[\mathcal{E}(\theta/T) + \mathcal{E}(\theta/2T)] \qquad (7)$$

In this equation, $\mathcal{E}(\theta/T)$ is the Einstein heat capacity function. This expression can adequately represent the heat capacity of some substances but has no strong basis in theory. Similar models which combine Debye and Einstein functions have been used to fit and extrapolate thermodynamic data [e.g., *Kelley et al.*, 1953; *Kelley*, 1929], but the Einstein functions used in such models are obtained by empirical fitting and have no direct physical meaning.

Tarasov [1950] modified the Debye theory to take account of specific structural features of crystals, such as molecular, chain, or layer groups. His work was extended to a number of highly anisotropic monatomic lattices (Se, Te, Hg, In, Zn, Cd, Sb, white Sn, and Li) by *De Sorbo* [1954]. *Newell* [1955] reexamined the theoretical basis of the Tarasov models for lamellar crystals and found that the predicted behavior ($C_V \propto T^2$ at low temperatures) implied special properties of the molecular forces other than those to be expected simply from the lamellar structure. He considered it unlikely that a general simple semiphenomenological law could be found for lamellar crystals comparable to the generality of the Debye law for isotropic materials.

Spectroscopists have frequently represented complex spectra by separating the vibrations of a chosen unit cell or 'molecule' of a substance into a discrete 'intramolecular' spectrum of Einstein oscillators plus an acoustic spectrum of 'translational' motions of the molecule (as discussed in paper 2). The model is illustrated here by referring to the calculations for quartz by *Lord and Morrow* [1957]. In the spectroscopic method the assignment of Einstein oscillators to the optic vibrations requires a detailed compilation of vibrational frequencies and degeneracies from an assumed lattice model for which the vibrating unit of the crystal is specified [e.g., *Raman*, 1943, 1961; *Saksena*, 1961]. *Lord and Morrow* [1957] assume that the fundamental vibrating unit in quartz is the unit cell, consisting of three SiO_2 groups. Each unit cell contributes 27 degrees of freedom to the total for the crystal. They assign the following wave numbers $w = (\omega/2\pi c)$ and species to the $\mathbf{K} = 0$ vibrations of quartz observed by infrared and Raman spectroscopy: species A, 207, 356, 466, and 1082 cm^{-1}; species B, 365, 520, 780, and 1055 cm^{-1}; and species E, 128, 264, 397, 452, 695, 800, 1064, and 1160 cm^{-1}. Species E vibrations are doubly degenerate. These frequencies account for 24 degrees of freedom and, correspondingly, 24 Einstein oscillators. According to the rationale discussed in the earlier part of this section the remaining 3 degrees of freedom are assumed to be translational motions of the unit cell. These 3 degrees of freedom obey a Debye frequency distribution law with a Debye temperature of 254°K, appropriate to one ninth of the degrees of freedom. The Debye temperature was determined from experimental heat capacities below 10°K. The frequency spectrum constructed in this way (schematically illustrated in Figure 3*d*, where it is to be compared with the spectrum proposed in this paper) leads to good agreement between observed and calculated heat capacities for quartz except at very low temperatures, where the specific heat is most senstitive to details of the spectrum.

The spectroscopic model is basically a powerful approach to modeling the vibrational spectra of minerals and, thereby, calculating the thermodynamic functions, for it enumerates the individual weighted frequencies $\omega_i^2(\mathbf{K} = 0)$. It does ignore variations of $\omega_i^2(\mathbf{K})$ with $\mathbf{K}$, coupling between oscillators, and anisotropy and dispersion in the acoustic branches. These problems limit its accuracy, especially at low temperatures. However, the main limitation for minerals is the simple fact that a complete enumeration of vibrational frequencies $\omega_i^2(\mathbf{K} = 0)$ and their weighting functions is generally not available for substances of geological and geophysical interest. The model proposed in the following section is less rigorous than lattice dynamical models based on interatomic forces and is less specific than the spectroscopic model, but it is generally useful for minerals with data currently available.

3. Formulation of Simplified Model for Complex Substances

The purpose of this work is to formulate the simplest vibrational spectrum that will predict the thermodynamic functions of minerals to an accuracy useful in geophysics and petrology. In this section a model is proposed for the lattice vibrational spectrum $g(\omega)$. The model proposed is consistent with lattice dynamics and is sufficiently detailed in its assumptions about the distribution of modes that the functions are closely specified. The model incorporates the four effects postulated in paper 1 as causes of the specific heat variations from a Debye model: anisotropy, dispersion, and low- and high-frequency optic modes. The model is consistent with lattice dynamics in requiring the use of the primitive unit cell, in correctly enumerating acoustic modes, and in recognizing anisotropy and dispersion of acoustic branches. It is more detailed than the spectroscopic model in the description of anisotropy and dispersion in the acoustic branches. It is less rigorous than the spectroscopic model because details about the distribution of optic modes are ignored. The success of the method results from the insensitivity of the thermodynamic functions to details of the spectrum at most frequencies characteristic of the optic modes.

Cell Parameters

It is a requirement of lattice dynamical theory that the primitive unit cell be taken as the fundamental vibrating unit of the crystal. A molecule of the crystal is here taken as the unit on which the chemical formula is based. The number of molecules in a unit cell is designated by Z, the number of atoms in a molecule by n, and the number of particles in a unit cell by s; hence $s = nZ$. There are $3s$ degrees of freedom associated with the unit cell and $3nN_A$ degrees of freedom associated with one mole of the substance. The unit cell volume is designated as V_L and the Brillouin zone volume is therefore $(2\pi)^3/V_L$. For simplicity the Brillouin zone is replaced by a sphere of the same volume with radius K_{max}. The volume of the Brillouin zone, V_R, is then

$$V_R = (2\pi)^3/V_L = N_A(2\pi)^3/ZV = \tfrac{4}{3}\pi K_{max}^3 \qquad (8a)$$

$$K_{max} = 2\pi(3N_A/4\pi ZV)^{1/3} \qquad (8b)$$

Equation (8*b*) defines the Brillouin zone boundary K_{max} and is consistent with the requirement of the Born theory that the same Brillouin zone be used for all waves (longitudinal and transverse). The shortest wavelength then which can propagate through the crystal, λ_{min}, is

$$\lambda_{min} = 2\pi/K_{max} = (4\pi VZ/3N_A)^{1/3} \qquad (9)$$

Acoustic Modes

Three of the $3s$ degrees of freedom must be acoustic modes. Each acoustic branch may be characterized at long wavelengths ($K \to 0$) by a directionally averaged sound velocity u_1, u_2 (shear branches), or u_3 (longitudinal branch). As was dis-

cussed in paper 1, rigorous calculation of $g(\omega)$ for each acoustic branch requires the directional average

$$u_i = \frac{1}{4\pi} \int_{\theta,\phi} \frac{d\Omega}{v_i^3(\theta, \phi)} \qquad i = 1, 2, 3 \tag{10}$$

Directional acoustic velocities $v_i(\theta, \phi)$ are generally not available for minerals; a procedure for estimating the directional averages from partial single-crystal data or from polycrystalline data was given in the appendix of paper 1.

In the model proposed here the frequency distribution $g(\omega)$ for the acoustic part of the spectrum is obtained from an assumed form for the dispersion curves for the three acoustic branches. For simplicity, a simple sinusoidal dispersion relation is used. This form is rigorously appropriate to linear lattices and represents empirically the approximate form found for many of the measured curves (see paper 2):

$$\omega_i(K) = \omega_{i,\max}(K) \sin\left(\frac{K}{K_{\max}} \cdot \frac{\pi}{2}\right) \tag{11}$$

where $\omega_{i,\max}$ is the maximum frequency reached at the zone boundary by branch i.

The branch distribution functions $g_i(\omega)$ are determined by summing the allowed wave vectors over the Brillouin zone. If the vibrational states of the crystal correspond to wave vectors K whose tips are uniformly distributed in reciprocal space, the density of vibrational states has the form

$$f_i(K)\, dK = 4\pi K^2\, dK \cdot d_i \tag{12a}$$

where d_i is the density, assumed to be uniform, of vibrational states in reciprocal space. (Compare with Debye theory, (4) in paper 1.) When this equation is expressed in terms of the vibrational frequency, it becomes

$$g_i(\omega_i)\, d\omega_i = f_i[K(\omega_i)] \frac{dK}{d\omega_i} d\omega_i = a_i \omega_i^2\, d\omega_i \tag{12b}$$

where from (11)

$$K = \frac{2}{\pi} K_{\max} \sin^{-1}\left(\frac{\omega_i(K)}{\omega_{i,\max}(K)}\right) \tag{13}$$

and therefore

$$\frac{dK}{d\omega_i} = \frac{2}{\pi} K_{\max}(\omega_{i,\max}^2 - \omega_i^2)^{-1/2} \tag{14}$$

The slope of each acoustic branch is required to approach the acoustic sound speed at $K = 0$:

$$d\omega_i/dK \to v_i \qquad \text{as } K \to 0 \qquad \omega_i \to 0 \tag{15}$$

The maximum frequency of each acoustic branch $\omega_{1,\max}$, $\omega_{2,\max}$, or $\omega_{3,\max}$ is given by

$$\omega_{i,\max} = v_i K_{\max} \cdot (2/\pi) \tag{16}$$

where $K_{\max}$ is given by (8b).

The value of a_i in (12b) is determined by the density of vibrational states in reciprocal space. As for the Debye theory discussed in paper 1 it is assumed that all normal modes of the crystal are represented by wave vectors within one reciprocal cell because only those vibrational modes are physically distinct. Each acoustic branch i accounts for $1/3s$ of the total degrees of freedom or for $3nN_A/3s = N_A/Z$ degrees of freedom for a crystal containing 1 gram molecular weight of formula units. The molar density d_i of vibrational states in reciprocal space is thus

$$d_i = \frac{N_A}{ZV_R} = \frac{V_L N_A}{Z(2\pi)^3} = \frac{V}{(2\pi)^3} \qquad i = 1, 2, 3$$

The acoustic spectral distribution is therefore obtained from (11)–(16) as

$$g(\omega)\, d\omega = \sum_{i=1}^{3} \frac{3N_A(2/\pi)^3[\sin^{-1}(\omega/\omega_i)]^2}{Z(\omega_i^2 - \omega^2)^{1/2}}\, d\omega \tag{17}$$

where the awkward notation $\omega_{i,\max}$ is replaced with ω_i to denote the maximum frequency for each acoustic branch.

The assumed sine wave dispersion for the acoustic branches causes singularities in $g(\omega)\, d\omega$ at ω_1, ω_2, and ω_3. Because the area under $g(\omega)$ is finite, the singularities in $g(\omega)$ do not give rise to any singularities in the thermodynamic functions.

Optic Modes

Experimental data do not yet provide detailed optic mode distributions of most minerals, and theoretical models fail to predict optic mode distributions accurately because of the lack of detailed descriptions of interatomic forces. However, because the thermodynamic functions are integrals over the frequency distribution, they are insensitive to details of the spectrum. For this reason, in the model proposed here the optic modes are described in the simplest way which satisfies experimental observations of the minimum and maximum values of vibrational frequencies; this description in general provides adequate accuracy to describe the thermodynamic functions.

There are total of $3s - 3$ optic modes per unit cell. Although in principle as many as $3s - 3$ separate optic modes could be identified and enumerated, in practice, only one or two groups of modes can be enumerated. They are usually stretching modes, e.g., the internal Si-O stretching modes and the Al-O stretching modes. If the stretching modes of one or two types of molecular groups can be identified, they are represented in the model by weighted Einstein oscillators. (They would be most accurately represented by a band of frequencies, but if single Einstein functions are used for the highest frequency modes, the errors introduced into heat capacity calculations are small if the modes do not represent more than about 25% of the total degrees of freedom. For example, in quartz the difference in heat capacity between a model with a single Einstein oscillator containing 22% of the modes at 1100 cm^{-1} and a model with the same number spread over a band between 1060 and 1172 cm^{-1} is less than 1% in the range 0° to 700°K). The model is presented here with only one stretching mode in order to avoid notational complexities, but the extension to two or more Einstein oscillators is obvious and has been used for some of the minerals studied. The stretching mode is represented by an Einstein oscillator at frequency ω_E, and the proportion of vibrational modes at this frequency is denoted as q. The density of states for the Einstein oscillator will be denoted as g_E and can be represented by the Dirac delta function δ:

$$g_E = 3qN_A n\delta(\omega - \omega_E) \tag{18}$$

The remaining $3s[1 - (1/s) - q]$ modes per unit cell or $3s[1 - (1/s) - q]\, nN_A$ modes per mole are assumed to be distributed uniformly over a range of frequencies spanning the spectrum between a lower limit ω_l and an upper limit ω_u. This uniformly distributed band of frequencies will be called the 'optic continuum' and will be designated as g_o. The density of states of this continuum (its height) is evaluated by requiring the total num-

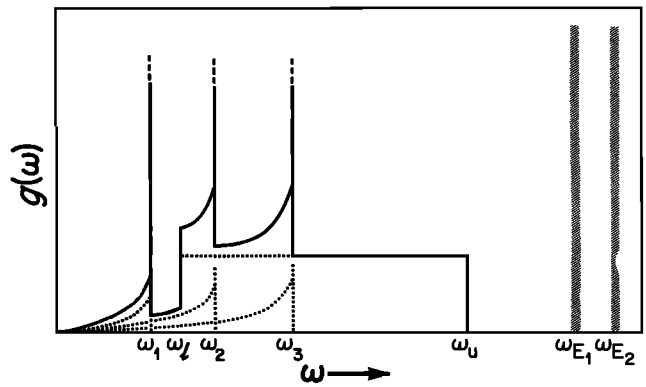

Fig. 1. Schematic model vibrational spectrum proposed in this paper for minerals. The singularities in the acoustic branches at ω_1, ω_2, and ω_3 are indicated by three dots on each branch. The dotted curves represent the acoustic branches and optical continuum separately. The solid curve is the total spectrum.

ber of degrees of freedom for 1 gram molecular weight of the crystal to be $3nN_A$:

$$g_o = 0 \qquad \omega < \omega_l \quad \omega > \omega_u$$
$$g_o = \frac{3N_An[1 - (1/s) - q]}{(\omega_u - \omega_l)} \qquad \omega_l < \omega < \omega_u \tag{19a}$$

In this representation, ω_l represents the lowest extent of the optical modes. As was mentioned in paper 2, this may not be the same frequency as that observed in Raman or far-infrared spectra taken at $K = 0$. In fact, the modes at $K = K_{max}$ are more important in thermodynamic calculations because of the K^2 weighting factor (equation (12a)). Therefore it is assumed that the lowest optical mode obeys the following dispersion law across the Brillouin zone:

$$\omega(K_{max}) = \omega(K = 0)/(1 + m_2/m_1)^{1/2} \tag{19b}$$

where m_1 and m_2 are the masses of the heaviest and lightest vibrating units, respectively, at low frequencies. These are specified in Table 6 of paper 2.

Summary of Vibrational Mode Distribution

The proposed vibrational spectra (shown schematically in Figure 1) consist of three acoustic branches, an optic continuum, and an Einstein oscillator(s) (optional), which are given by (17), (18), and (19):

$$g(\omega) = \begin{cases} \sum_{i=1}^{3} 3N_A\left(\frac{2}{\pi}\right)^3 \frac{1}{Z} \frac{[\sin^{-1}(\omega/\omega_i)]^2}{(\omega_i^2 - \omega^2)^{1/2}} + g_0(\omega)^* & \\ & 0 < \omega < \omega_1 \\ \sum_{i=2}^{3} 3N_A\left(\frac{2}{\pi}\right)^3 \frac{1}{Z} \frac{[\sin^{-1}(\omega/\omega_i)]^2}{(\omega_i^2 - \omega^2)^{1/2}} + g_o & \\ & \omega_1 < \omega < \omega_2 \\ 3N_A\left(\frac{2}{\pi}\right)^3 \frac{1}{Z} \frac{[\sin^{-1}(\omega/\omega_3)]^2}{(\omega_3^2 - \omega^2)^{1/2}} + g_o & \omega_2 < \omega < \omega_3 \\ g_o & \omega > \omega_3 \\ g_o + g_E & \omega = \omega_E \end{cases} \tag{20}$$

The asterisk means that it is implicit henceforth that g_o is zero outside of the bounds $\omega_l < \omega < \omega_u$.

Thermodynamic Functions

The total molar specific heat normalized to the monatomic equivalent, C_V^*, then becomes

$$C_V^* = \frac{3N_Ak}{nZ}\left(\frac{2}{\pi}\right)^3 \cdot \sum_{i=1}^{3} \int_0^{\omega} \frac{[\sin^{-1}(\omega/\omega_i)]^2(\hbar\omega/kT)^2 \exp(\hbar\omega/kT) d\omega}{(\omega_i^2 - \omega^2)^{1/2}[\exp(\hbar\omega/kT) - 1]^2}$$
$$+ 3N_Ak\left(1 - \frac{1}{s} - q\right) \int_{\omega_l}^{\omega_u} \frac{(\hbar\omega/kT)^2 \exp(\hbar\omega/kT)\, d\omega}{(\omega_u - \omega_l)[\exp(\hbar\omega/kT) - 1]^2}$$
$$+ \frac{3N_Akq(\hbar\omega_E/kT) \exp(\hbar\omega_E/kT)}{[\exp(\hbar\omega_E/kT) - 1]^2} \tag{21}$$

where $N_Ak = R$, the gas constant, and $nZ = s$, the number of atoms in the unit cell.

This expression contains three functions which are similar to the Debye function:

'Dispersed acoustic function'

$$\mathcal{S}(x_l) = \left(\frac{2}{\pi}\right)^3 \int_0^{x_l} \frac{[\sin^{-1}(x/x_l)]^2 x^2 e^x\, dx}{(x_l^2 - x^2)^{1/2}(e^x - 1)^2} \tag{22}$$

'Optic continuum function'

$$\mathcal{K}\left(\frac{x_u}{x_l}\right) = \int_{x_l}^{x_u} \frac{x^2 e^x\, dx}{(x_u - x_l)(e^x - 1)^2} \tag{23}$$

Einstein function

$$\mathcal{E}(x_E) = x_E^2\, e^{x_E}/(e^{x_E} - 1)^2 \tag{24}$$

In these expressions, $x = \hbar\omega/kT$. $\mathcal{S}(x_l)$ is the heat capacity function for a monatomic solid which has a sine dispersion function;

$$\mathcal{K}\left(\frac{x_u}{x_l}\right)$$

is the heat capacity function of a continuum spanning the range (of nondimensionalized frequencies) from x_l to x_u; $\mathcal{E}(x_E)$ is the heat capacity function of an Einstein oscillator. These functions are given in Tables 1, 2, and 3. At low temperatures the dispersed acoustic function has the same dependence on the third power of the temperature as the Debye function.

In terms of these functions the molar heat capacity, normalized to the monatomic equivalent, is

$$C_V^* = \frac{3N_Ak}{nZ} \sum_{i=1}^{3} \mathcal{S}(x_i) + 3N_Ak\left(1 - \frac{3}{3s} - q\right) \mathcal{K}\left(\frac{x_u}{x_l}\right)$$
$$+ 3N_Akq\, \mathcal{E}(x_E) \tag{25}$$

It is most important to emphasize that the heat capacity can be calculated from the tables of these functions just as it can be calculated from tables of the Debye or Einstein functions. As an example of the use of the tables, consider the heat capacity of quartz at 300°K. Spectral data give $w_l = 128\ cm^{-1}$, $w_u = 809\ cm^{-1}$, and $w_E = 1100\ cm^{-1}$. Mode enumeration gives 0.22 modes in the Si-O stretching band, represented by an Einstein oscillator at 1100 cm^{-1}. The nondimensionalized frequencies are $x_l = 0.61$, $x_u = 3.88$, and $x_E = 5.28$. From (8) and (16) the maximum frequencies of the three acoustic branches are $w_{1,max} = 103\ cm^{-1}$, $w_{2,max} = 122\ cm^{-1}$, and $w_{3,max} = 165\ cm^{-1}$, giving

TABLE 1. Dispersed Sine Function (22)

x_i	$S(x_i)$	x_i	$S(x_i)$	x_i	$S(x_i)$	x_i	$S(x_i)$
0.1	0.999323	5.1	0.245435	10.1	0.027960	15.1	0.006660
0.2	0.997321	5.2	0.234640	10.2	0.026954	15.2	0.006514
0.3	0.993989	5.3	0.224270	10.3	0.025993	15.3	0.006373
0.4	0.989350	5.4	0.214316	10.4	0.025075	15.4	0.006236
0.5	0.983426	5.5	0.204767	10.5	0.024199	15.5	0.006103
0.6	0.976248	5.6	0.195613	10.6	0.023362	15.6	0.005974
0.7	0.967853	5.7	0.186844	10.7	0.022563	15.7	0.005849
0.8	0.958282	5.8	0.178448	10.8	0.021798	15.8	0.005727
0.9	0.947583	5.9	0.170413	10.9	0.021068	15.9	0.005609
1.0	0.935806	6.0	0.162728	11.0	0.020369	16.0	0.005494
1.1	0.923010	6.1	0.155382	11.1	0.019700	16.1	0.005383
1.2	0.909254	6.2	0.148363	11.2	0.019060	16.2	0.005274
1.3	0.894601	6.3	0.141659	11.3	0.018448	16.3	0.005169
1.4	0.879119	6.4	0.135259	11.4	0.017861	16.4	0.005066
1.5	0.862873	6.5	0.129151	11.5	0.017299	16.5	0.004966
1.6	0.845933	6.6	0.123324	11.6	0.016761	16.6	0.004869
1.7	0.828371	6.7	0.117767	11.7	0.016245	16.7	0.004775
1.8	0.810258	6.8	0.112470	11.8	0.015750	16.8	0.004683
1.9	0.791662	6.9	0.107420	11.9	0.015275	16.9	0.004593
2.0	0.772656	7.0	0.102609	12.0	0.014819	17.0	0.004506
2.1	0.753306	7.1	0.098025	12.1	0.014382	17.1	0.004421
2.2	0.733681	7.2	0.093659	12.2	0.013962	17.2	0.004338
2.3	0.713846	7.3	0.089502	12.3	0.013559	17.3	0.004257
2.4	0.693864	7.4	0.085543	12.4	0.013171	17.4	0.004179
2.5	0.673795	7.5	0.081775	12.5	0.012799	17.5	0.004102
2.6	0.653698	7.6	0.078188	12.6	0.012440	17.6	0.004028
2.7	0.633628	7.7	0.074775	12.7	0.012096	17.7	0.003955
2.8	0.613635	7.8	0.071526	12.8	0.011764	17.8	0.003884
2.9	0.593769	7.9	0.068434	12.9	0.011445	17.9	0.003814
3.0	0.574074	8.0	0.065492	13.0	0.011137	18.0	0.003747
3.1	0.554592	8.1	0.062693	13.1	0.010841	18.1	0.003681
3.2	0.535361	8.2	0.060029	13.2	0.010556	18.2	0.003616
3.3	0.516415	8.3	0.057495	13.3	0.010281	18.3	0.003553
3.4	0.497785	8.4	0.055083	13.4	0.010015	18.4	0.003492
3.5	0.479501	8.5	0.052788	13.5	0.009759	18.5	0.003432
3.6	0.461585	8.6	0.050604	13.6	0.009513	18.6	0.003373
3.7	0.444060	8.7	0.048525	13.7	0.009274	18.7	0.003316
3.8	0.426943	8.8	0.046547	13.8	0.009044	18.8	0.003260
3.9	0.410252	8.9	0.044664	13.9	0.008822	18.9	0.003206
4.0	0.393997	9.0	0.042871	14.0	0.008607	19.0	0.003153
4.1	0.378190	9.1	0.041164	14.1	0.008400	19.1	0.003100
4.2	0.362838	9.2	0.039539	14.2	0.008199	19.2	0.003049
4.3	0.347947	9.3	0.037991	14.3	0.008005	19.3	0.003000
4.4	0.333520	9.4	0.036517	14.4	0.007817	19.4	0.002951
4.5	0.319558	9.5	0.035112	14.5	0.007636	19.5	0.002903
4.6	0.306061	9.6	0.033773	14.6	0.007460	19.6	0.002857
4.7	0.293028	9.7	0.032497	14.7	0.007289	19.7	0.002811
4.8	0.280454	9.8	0.031281	14.8	0.007125	19.8	0.002767
4.9	0.268334	9.9	0.030121	14.9	0.006965	19.9	0.002723
5.0	0.256664	10.0	0.029015	15.0	0.006810	20.0	0.002680

$x_{i,\max}$ for the acoustic branches of 0.49, 0.59, and 0.79. Note from Table 1 that at room temperature the acoustic branches are nearly saturated ($x \sim 0$) and contribute nearly the value of the Dulong-Petit limit, normalized to $3/3s$ degrees of freedom. Thus the three acoustic branches contribute 0.65 cal mol^{-1} °K^{-1} to C_V*. From Table 2 the continuum contributes $(1 - 3/27 - 0.22) \times 3.90 = 2.63$ cal mol^{-1} °K^{-1}. From Table 3 the Einstein oscillator contributes $0.84 \times 0.22 = 0.185$ cal mol^{-1} °K^{-1}. The total calculated C_V* at 300°K is therefore 3.47 cal mol^{-1} °K^{-1}. For comparison, C_V* from experimental data is 3.54 cal mol^{-1} °K^{-1}.

Expressions for the entropy, the internal energy, and the Helmholtz free energy may be derived from Table 1 in paper 1:

Internal energy in excess of that at 0°K

$$E^* = \frac{3N_A kT}{nZ}\left(\frac{2}{\pi}\right)^3 \sum_{i=1}^{3} \int_0^{x_i} \frac{[\sin^{-1}(x/x_i)]^2\, x\, dx}{(x_i^2 - x^2)^{1/2}(e^x - 1)} + 3N_A kT\left(1 - \frac{3}{3s} - q\right)\int_{x_i}^{x_u} \frac{x\, dx}{(x_u - x_i)(e^x - 1)} + \frac{3N_A kTqx_E}{(e^{x_E} - 1)} \tag{26}$$

Entropy, Third law

$$S^* = \frac{3N_A k\left(\frac{2}{\pi}\right)^3}{nZ} \sum_{i=1}^{3} \int_0^{x_i} \frac{[\sin^{-1}(x/x_i)]^2 x\, dx}{(x_i^2 - x^2)^{1/2}(e^x - 1)} - \frac{3N_A k}{nZ}\left(\frac{2}{\pi}\right)^3 \sum_{i=1}^{3} \int_0^{x_i} \frac{[\sin^{-1}(x/x_i)]^2}{(x_i^2 - x^2)^{1/2}} \ln(1 - e^{-x})\, dx + 3N_A k\left(1 - \frac{3}{3s} - q\right)\int_{x_i}^{x_u} \frac{x\, dx}{(e^x - 1)} - 3N_A k\left(1 - \frac{3}{3s} - q\right)\int_{\epsilon}^{x_u} \ln(1 - e^{-x})\, dx + \frac{3N_A kqx_E}{(e^{x_E} - 1)} - 3N_A kq \ln(1 - e^{-x_E}) \tag{27}$$

Helmholtz free energy, above that at 0°K

$$F^* = \frac{3N_A kT}{nZ}\left(\frac{2}{\pi}\right)^3 \sum_{i=1}^{3} \int_0^{x_i} \frac{[\sin^{-1}(x/x_i)]^2 \ln(1 - e^{-x})\, dx}{(x_i^2 - x^2)^{1/2}}$$

TABLE 2. Continuum Function (23)

x_u \ x_l	0.1	0.2	0.3	0.4	0.5	0.6	0.7	0.8	0.9	1.0
0.5	0.991452	0.989251	0.986507	0.983228						
1.0	0.970066	0.966567	0.962543	0.958002	0.952957	0.947420	0.941407	0.934932	0.928014	
1.5	0.937303	0.932629	0.927454	0.921787	0.915644	0.909037	0.901984	0.894502	0.886611	0.878330
2.0	0.895655	0.889966	0.883803	0.877179	0.870109	0.862610	0.854697	0.846392	0.837715	0.828685
2.5	0.847944	0.841417	0.834447	0.827051	0.819242	0.811038	0.802459	0.793524	0.784254	0.774670
3.0	0.796922	0.789739	0.782147	0.774160	0.765798	0.757077	0.748017	0.738637	0.728961	0.719008
3.5	0.744989	0.737320	0.729275	0.720872	0.712127	0.703059	0.693687	0.684032	0.674117	0.663961
4.0	0.694023	0.686023	0.677679	0.669009	0.660031	0.650765	0.641228	0.631443	0.621430	0.611211
4.5	0.645361	0.637159	0.628645	0.619837	0.610752	0.601410	0.591829	0.582031	0.572036	0.561865
5.0	0.599836	0.591539	0.582961	0.574117	0.565025	0.555705	0.546176	0.536458	0.526570	0.516534
5.5	0.557876	0.549571	0.541010	0.532211	0.523190	0.513968	0.504562	0.494991	0.485277	0.475438
6.0	0.519609	0.511360	0.502890	0.494185	0.485293	0.476223	0.466992	0.457619	0.448124	0.438527
6.5	0.484955	0.476810	0.468456	0.459910	0.451188	0.442308	0.433288	0.424147	0.414902	0.405573
7.0	0.453706	0.445701	0.437506	0.429139	0.420614	0.411950	0.403164	0.394274	0.385298	0.376252
7.5	0.425589	0.417747	0.409733	0.401564	0.393254	0.384822	0.376283	0.367655	0.358955	0.350200
8.0	0.400301	0.392637	0.384818	0.376857	0.368773	0.360579	0.352293	0.343931	0.335510	0.327045
8.5	0.377539	0.370062	0.362444	0.354699	0.346843	0.338890	0.330857	0.322760	0.314614	0.306435
9.0	0.357014	0.349730	0.342316	0.334787	0.327158	0.319445	0.311661	0.303824	0.295947	0.288046
9.5	0.338464	0.331372	0.324161	0.316847	0.309443	0.301963	0.294423	0.286838	0.279222	0.271589
10.0	0.321652	0.314750	0.307740	0.300635	0.293450	0.286198	0.278894	0.271552	0.264186	0.256810
10.5	0.306368	0.299652	0.292838	0.285937	0.278964	0.271932	0.264856	0.257747	0.250621	0.243491
11.0	0.292428	0.285895	0.279270	0.272567	0.265799	0.258979	0.252120	0.245235	0.238338	0.231441
11.5	0.279675	0.273318	0.266877	0.260364	0.253792	0.247175	0.240524	0.233853	0.227174	0.220499
12.0	0.267970	0.261783	0.255518	0.249189	0.242805	0.236382	0.229930	0.223462	0.216990	0.210526
12.5	0.257194	0.251171	0.245076	0.238921	0.232719	0.226481	0.220218	0.213943	0.207668	0.201404
13.0	0.247244	0.241378	0.235446	0.229459	0.223429	0.217367	0.211285	0.205194	0.199106	0.193032
13.5	0.238030	0.232315	0.226539	0.220713	0.214848	0.208954	0.203044	0.197128	0.191218	0.185323
14.0	0.229475	0.223906	0.218279	0.212606	0.206898	0.201165	0.195418	0.189669	0.183927	0.178203
14.5	0.221512	0.216081	0.210598	0.205072	0.199513	0.193934	0.188343	0.182751	0.177170	0.171608
15.0	0.214081	0.208784	0.203438	0.198051	0.192636	0.187203	0.181760	0.176320	0.170890	0.165482
15.5	0.207132	0.201963	0.196747	0.191495	0.186217	0.180923	0.175622	0.170324	0.165040	0.159778
16.0	0.200620	0.195572	0.190483	0.185359	0.180211	0.175050	0.169883	0.164723	0.159576	0.154453
16.5	0.194503	0.189573	0.184604	0.179603	0.174580	0.169546	0.164508	0.159478	0.154462	0.149471
17.0	0.188749	0.183931	0.179077	0.174193	0.169290	0.164377	0.159462	0.154556	0.149665	0.144801
17.5	0.183325	0.178616	0.173871	0.169100	0.164311	0.159514	0.154716	0.149929	0.145158	0.140413
18.0	0.178204	0.173598	0.168960	0.164296	0.159616	0.154930	0.150245	0.145570	0.140914	0.136234
18.5	0.173361	0.168855	0.164318	0.159757	0.155183	0.150602	0.146025	0.141458	0.136910	0.132390
19.0	0.168774	0.164364	0.159924	0.155463	0.150939	0.146510	0.142035	0.137572	0.133129	0.128713
19.5	0.164425	0.160106	0.155759	0.151393	0.147015	0.142634	0.138258	0.133894	0.129550	0.125234
20.0	0.160293	0.156062	0.151806	0.147531	0.143246	0.138958	0.134676	0.130407	0.126159	0.121939
20.5	0.156364	0.152219	0.148049	0.143861	0.139665	0.135467	0.131275	0.127098	0.122941	0.118812
21.0	0.152624	0.148560	0.144473	0.140370	0.136259	0.132147	0.128042	0.123952	0.119883	0.115843
21.5	0.149058	0.145073	0.141066	0.137044	0.133015	0.128987	0.124965	0.120959	0.116974	0.113017
22.0	0.145656	0.141747	0.137817	0.133873	0.129923	0.125974	0.122032	0.118107	0.114202	0.110327
22.5	0.142406	0.138570	0.134714	0.130845	0.126971	0.123099	0.119234	0.115386	0.111560	0.107762
23.0	0.139298	0.135532	0.131748	0.127952	0.124151	0.120352	0.116562	0.112788	0.109036	0.105314
23.5	0.136324	0.132626	0.128910	0.125184	0.121453	0.117725	0.114007	0.110305	0.106625	0.102974
24.0	0.133474	0.129842	0.126193	0.122533	0.118871	0.115211	0.111562	0.107929	0.104318	0.100736
24.5	0.130742	0.127173	0.123588	0.119993	0.116396	0.112803	0.109219	0.105653	0.102109	0.098594
25.0	0.128119	0.124611	0.121089	0.117557	0.114023	0.110493	0.106974	0.103471	0.099992	0.096541
25.5	0.125601	0.122152	0.118689	0.115217	0.111744	0.108276	0.104818	0.101378	0.097960	0.094572
26.0	0.123180	0.119788	0.116383	0.112970	0.109556	0.106147	0.102749	0.099368	0.096010	0.092681
26.5	0.120851	0.117514	0.114165	0.110808	0.107451	0.104100	0.100759	0.097436	0.094136	0.090865
27.0	0.118609	0.115326	0.112031	0.108728	0.105426	0.102130	0.098845	0.095578	0.092334	0.089118
27.5	0.116450	0.113218	0.109975	0.106725	0.103476	0.100234	0.097003	0.093790	0.090599	0.087437
28.0	0.114367	0.111185	0.107993	0.104795	0.101597	0.098407	0.095228	0.092067	0.088929	0.085819
28.5	0.112359	0.109225	0.106082	0.102933	0.099785	0.096645	0.093516	0.090406	0.087318	0.084259
29.0	0.110420	0.107333	0.104237	0.101136	0.099037	0.094945	0.091865	0.088804	0.085765	0.082755
29.5	0.108547	0.105505	0.102455	0.099401	0.096349	0.093304	0.090271	0.087258	0.084266	0.081303
30.0	0.106736	0.103739	0.100733	0.097724	0.094717	0.091718	0.088732	0.085764	0.082818	0.079901

$$+ \frac{3N_A kT\left(1 - \frac{3}{3s} - q\right)}{(x_u - x_l)} \int_{x_l}^{x_u} \ln(1 - e^{-x})\, dx$$

$$+ 3N_A kTq \ln(1 - e^{-x_\varepsilon}) \qquad (28)$$

4. Data Required for Model

The model proposed in section 3 allows calculation of the thermodynamic functions from the following acoustic and spectroscopic data: (1) three acoustic velocities u_1, u_2, and u_3 from which the acoustic cutoff frequencies ω_1, ω_2, and ω_3 (or w_1, w_2, and w_3) are calculated from (8) and (16) (acoustic data are given in Table 4); (2) two spectral frequencies ω_l and ω_u (or w_l and w_u) which define the limits of the optic continuum (spectral data are given in Table 5); and (3) frequencies and partitioning fractions for any intramolecular modes separated from the optic continuum (Table 5).

The model is demonstrated in this paper with calculations of the temperature dependence of the heat capacity for several simple substances and framework silicates; chain silicates and orthosilicates will be considered in paper 4 (S. W. Kieffer, unpublished manuscript, 1979). The temperature and pressure dependence of the internal energy, heat capacity, entropy, and Helmholtz free energy will be given in paper 5 (S. W. Kieffer, unpublished manuscript, 1979).

Specific heat data for minerals at atmospheric pressure are usually measured and tabulated in terms of C_P, the specific heat at constant pressure, rather than in terms of C_V, the quantity calculated by (25). C_P and C_V are related by

$$C_V = C_P - TV\epsilon^2 B \qquad (29)$$

TABLE 2. (continued)

x_u \ x_ℓ	1.1	1.2	1.3	1.4	1.5	1.6	1.7	1.8	1.9	2.0
0.5										
1.0										
1.5	0.869681	0.850685	0.851365	0.841745						
2.0	0.819325	0.809657	0.799705	0.789491	0.779041	0.768377	0.757523	0.746504	0.735341	
2.5	0.764794	0.754651	0.744261	0.733650	0.722840	0.711855	0.700721	0.689458	0.678090	0.666639
3.0	0.708802	0.698364	0.687720	0.676891	0.665901	0.654773	0.643529	0.632193	0.620786	0.609331
3.5	0.653587	0.643018	0.632277	0.621386	0.610368	0.599246	0.588041	0.576775	0.565469	0.554145
4.0	0.600807	0.590240	0.579534	0.568708	0.557787	0.546791	0.535741	0.524658	0.513562	0.502473
4.5	0.551540	0.541082	0.530512	0.519851	0.509121	0.498343	0.487536	0.476720	0.465915	0.455137
5.0	0.506370	0.496099	0.485741	0.475318	0.464849	0.454353	0.443851	0.433360	0.422898	0.412484
5.5	0.465495	0.455468	0.445376	0.435240	0.425077	0.414907	0.404749	0.394618	0.384534	0.374511
6.0	0.428845	0.419099	0.409307	0.399488	0.389660	0.379841	0.370048	0.360297	0.350605	0.340987
6.5	0.396177	0.386734	0.377261	0.367776	0.358297	0.348840	0.339421	0.330056	0.320761	0.311548
7.0	0.367156	0.358027	0.348881	0.339736	0.330609	0.321515	0.312469	0.303486	0.294581	0.285766
7.5	0.341407	0.332594	0.323776	0.314969	0.306189	0.297452	0.288771	0.280161	0.271634	0.263203
8.0	0.318554	0.310053	0.301556	0.293080	0.284639	0.276247	0.267919	0.259667	0.251503	0.243439
8.5	0.298239	0.290042	0.281857	0.273700	0.265585	0.257526	0.249534	0.241624	0.233805	0.226089
9.0	0.280136	0.272232	0.264347	0.256497	0.248694	0.240950	0.233279	0.225692	0.218199	0.210812
9.5	0.263954	0.256331	0.248733	0.241175	0.233668	0.226224	0.218856	0.211574	0.204389	0.197309
10.0	0.249438	0.242083	0.234759	0.227477	0.220250	0.213090	0.206008	0.199013	0.192116	0.185326
10.5	0.236369	0.229269	0.222203	0.215184	0.208222	0.201329	0.194515	0.187791	0.181164	0.174644
11.0	0.224557	0.217699	0.210878	0.204106	0.197394	0.190753	0.184192	0.177720	0.171347	0.165081
11.5	0.213841	0.207212	0.200622	0.194084	0.187607	0.181203	0.174879	0.168545	0.162509	0.156479
12.0	0.204082	0.197669	0.191299	0.184981	0.178726	0.172543	0.166443	0.160432	0.154518	0.148710
12.5	0.195163	0.188955	0.182791	0.176681	0.170635	0.164662	0.158770	0.152969	0.147264	0.141663
13.0	0.186983	0.180968	0.175000	0.169086	0.163237	0.157461	0.151766	0.146161	0.140652	0.135246
13.5	0.179456	0.173625	0.167840	0.162112	0.156448	0.150858	0.145349	0.139928	0.134603	0.129379
14.0	0.172508	0.166850	0.161240	0.155687	0.150198	0.144783	0.139448	0.134201	0.129049	0.123997
14.5	0.166076	0.160583	0.155138	0.149750	0.144426	0.139177	0.134006	0.128924	0.123933	0.119042
15.0	0.160105	0.154768	0.149479	0.144247	0.139081	0.133937	0.128972	0.124043	0.119206	0.114467
15.5	0.154548	0.149358	0.144218	0.139134	0.134115	0.129169	0.124301	0.119518	0.114826	0.110229
16.0	0.149363	0.144313	0.139314	0.134371	0.129492	0.124685	0.119956	0.115311	0.110755	0.106294
16.5	0.144514	0.139598	0.134732	0.129922	0.125176	0.120502	0.115904	0.111390	0.106963	0.102629
17.0	0.139970	0.135181	0.130441	0.125758	0.121139	0.116590	0.112117	0.107726	0.103422	0.099209
17.5	0.135703	0.131034	0.126416	0.121853	0.117354	0.112924	0.108559	0.104296	0.100107	0.096009
18.0	0.131688	0.127135	0.122631	0.118183	0.113798	0.109481	0.105239	0.101077	0.096999	0.093009
18.5	0.127904	0.123460	0.119056	0.114727	0.110451	0.106242	0.102107	0.098051	0.094077	0.090191
19.0	0.124332	0.119993	0.115703	0.111468	0.107295	0.103190	0.099156	0.095201	0.091326	0.087538
19.5	0.120953	0.116714	0.112525	0.108389	0.104315	0.100307	0.096371	0.092511	0.088732	0.085037
20.0	0.117754	0.113610	0.109516	0.105476	0.101496	0.097582	0.093738	0.089970	0.086281	0.082675
20.5	0.114719	0.110667	0.106664	0.102715	0.098825	0.095000	0.091245	0.087564	0.083962	0.080441
21.0	0.111837	0.107873	0.103957	0.100095	0.096291	0.092552	0.088881	0.085284	0.081764	0.078324
21.5	0.109096	0.105216	0.101385	0.097605	0.093884	0.090227	0.086637	0.083120	0.079678	0.076316
22.0	0.106487	0.102688	0.098936	0.095236	0.091595	0.088016	0.084503	0.081063	0.077696	0.074408
22.5	0.103999	0.100278	0.096603	0.092980	0.089414	0.085910	0.082472	0.079105	0.075810	0.072593
23.0	0.101626	0.097978	0.094378	0.090828	0.087335	0.083903	0.080536	0.077239	0.074014	0.070865
23.5	0.099358	0.095782	0.092252	0.088773	0.085350	0.081988	0.078690	0.075460	0.072301	0.069217
24.0	0.097189	0.093682	0.090221	0.086810	0.083454	0.080158	0.076925	0.073760	0.070665	0.067644
24.5	0.095113	0.091672	0.088277	0.084931	0.081640	0.078408	0.075239	0.072136	0.069102	0.066141
25.0	0.093124	0.089747	0.086415	0.083132	0.079904	0.076733	0.073624	0.070581	0.067606	0.064703
25.5	0.091217	0.087901	0.084630	0.081408	0.078239	0.075128	0.072078	0.069092	0.066174	0.063326
26.0	0.089386	0.086129	0.082917	0.079754	0.076643	0.073589	0.070595	0.067665	0.064801	0.062007
26.5	0.087627	0.084428	0.081273	0.078165	0.075110	0.072111	0.069171	0.066295	0.063484	0.060742
27.0	0.085936	0.082792	0.079692	0.076639	0.073637	0.070692	0.067804	0.064980	0.062219	0.059527
27.5	0.084309	0.081218	0.078171	0.075171	0.072221	0.069327	0.066490	0.063715	0.061004	0.058359
28.0	0.082742	0.079703	0.076707	0.073758	0.070859	0.068014	0.065226	0.062499	0.059835	0.057237
28.5	0.081233	0.078244	0.075297	0.072397	0.069546	0.066749	0.064009	0.061329	0.058710	0.056156
29.0	0.079777	0.076836	0.073939	0.071085	0.068281	0.065531	0.062836	0.060201	0.057626	0.055116
29.5	0.078372	0.075479	0.072627	0.069820	0.067062	0.064356	0.061705	0.059114	0.056582	0.054113
30.0	0.077016	0.074168	0.071361	0.068598	0.065884	0.063222	0.060615	0.058065	0.055574	0.053146

where ϵ is the volume coefficient of thermal expansion, B is the bulk modulus, and V is the specific volume: ϵ, B, and V in general depend on the temperature. They were specified as a function of temperature T as follows:

$$\epsilon = \epsilon_0 + \epsilon_1 T + \epsilon_2 T^2$$
$$B = B_0 + (\partial B_0/\partial T)\Delta T \qquad (30)$$
$$V = V_0 + (\partial V_0/\partial T)\Delta T$$

where B_0 and V_0 are the values at 298°K. Values of the parameters were obtained from *Clark* [1966] or estimated from structural analogues. The correction from C_P to C_V is significant only at high temperatures ($T > 300$°K) for most minerals. (*Barron and Munn* [1968] have pointed out that $C_P - TV\epsilon^2 B$ is not a simple quantity for nonisotropic solids. It is actually the heat capacity defined under the double restraint of constant volume and isotropic stress. Corrections from this quantity to the heat capacity at constant strain are of the order of 1%.) At temperatures (~700°K) where the C_P-C_V correction is large (a few percent), anharmonic effects that are not considered in the model may be more important than the C_P-C_V correction (see discussion below). $(C_P - C_V)/C_P$ is generally less than 1% at 100°K and is about 4% at 700°K for silicate minerals. For halite the correction from C_P to C_V is large (~5%) even at room temperature; values of C_V for halite have been obtained from C_P data of *Raman* [1961] and *Janaff* [1965*a*, *b*, 1966, 1967].

For comparison with the predictions of the harmonic theory developed here, C_V thus obtained from C_P must be corrected to a fixed volume, e.g., the volume of the crystal at 0°K, because the theory has assumed that the effects of thermal expansion can be neglected, i.e., that volume is not a function of temperature and that the lattice vibrational spectrum is therefore not a function of temperature. In fact, thermal expansion has the effect of shifting the spectrum, to lower frequencies if the material expands as the temperature is raised.

TABLE 2. (continued)

x_u \ x_ℓ	2.1	2.2	2.3	2.4	2.5	2.6	2.7	2.8	2.9	3.0
0.5										
1.0										
1.5										
2.0										
2.5	0.655128	0.643578	0.632008	0.620439						
3.0	0.597847	0.586356	0.574876	0.563425	0.552023	0.540684	0.529425	0.518261	0.507204	
3.5	0.542820	0.531516	0.520249	0.509037	0.497897	0.486844	0.475892	0.465054	0.454343	0.443771
4.0	0.491410	0.480390	0.469429	0.458545	0.447752	0.437064	0.426495	0.416057	0.405761	0.395616
4.5	0.444407	0.433738	0.423148	0.412652	0.402262	0.391993	0.381856	0.371862	0.362021	0.352342
5.0	0.402132	0.391859	0.381679	0.371606	0.361653	0.351831	0.342151	0.332624	0.323257	0.314060
5.5	0.364565	0.354710	0.344959	0.335326	0.325823	0.316459	0.307244	0.298188	0.289299	0.280583
6.0	0.331456	0.322027	0.312711	0.303520	0.294465	0.285556	0.276802	0.268209	0.259787	0.251539
6.5	0.302431	0.293423	0.284535	0.275778	0.267161	0.258694	0.250385	0.242239	0.234265	0.226467
7.0	0.277053	0.268455	0.259981	0.251642	0.243446	0.235403	0.227518	0.219793	0.212248	0.204874
7.5	0.254879	0.246673	0.238595	0.230654	0.222859	0.215216	0.207732	0.200412	0.193262	0.186285
8.0	0.235485	0.227653	0.219950	0.212385	0.204966	0.197699	0.190590	0.183645	0.176867	0.170260
8.5	0.218486	0.211005	0.203655	0.196443	0.189376	0.182461	0.175702	0.169105	0.162673	0.156409
9.0	0.203538	0.196388	0.189368	0.182486	0.175748	0.169160	0.162727	0.156452	0.150339	0.144392
9.5	0.190345	0.183503	0.176792	0.170217	0.163786	0.157502	0.151370	0.145394	0.139577	0.133921
10.0	0.178651	0.172098	0.165674	0.159386	0.153238	0.147237	0.141384	0.135685	0.130141	0.124754
10.5	0.168239	0.161956	0.155800	0.149779	0.143895	0.138154	0.132561	0.127117	0.121825	0.116686
11.0	0.158928	0.152895	0.146989	0.141215	0.135577	0.130080	0.124726	0.119518	0.114459	0.109549
11.5	0.150562	0.144764	0.139091	0.133547	0.128137	0.122865	0.117733	0.112744	0.107900	0.103203
12.0	0.143013	0.137434	0.131978	0.126649	0.121451	0.116388	0.111462	0.106677	0.102032	0.097530
12.5	0.136173	0.130798	0.125544	0.120415	0.115414	0.110546	0.105812	0.101215	0.096756	0.092435
13.0	0.129948	0.124754	0.119699	0.114757	0.109941	0.105254	0.100699	0.096277	0.091989	0.087837
13.5	0.124262	0.119258	0.114369	0.109602	0.104958	0.100441	0.096051	0.091793	0.087665	0.083669
14.0	0.119050	0.114213	0.109491	0.104887	0.100403	0.096044	0.091810	0.087704	0.083725	0.079875
14.5	0.114255	0.109576	0.105009	0.100558	0.096226	0.092014	0.087926	0.083961	0.080122	0.076408
15.0	0.109830	0.105299	0.100878	0.096571	0.092380	0.088307	0.084355	0.080524	0.076815	0.073228
15.5	0.105734	0.101342	0.097059	0.092887	0.088829	0.084887	0.081062	0.077356	0.073769	0.070301
16.0	0.101932	0.097672	0.093518	0.089473	0.085540	0.081721	0.078016	0.074427	0.070955	0.067599
16.5	0.098393	0.094257	0.090226	0.086302	0.082486	0.078782	0.075190	0.071712	0.068347	0.065096
17.0	0.095092	0.091073	0.087158	0.083347	0.079642	0.076047	0.072562	0.069187	0.065924	0.062772
17.5	0.092005	0.088098	0.084291	0.080587	0.076988	0.073496	0.070110	0.066834	0.063666	0.060608
18.0	0.089112	0.085310	0.081607	0.078004	0.074505	0.071110	0.067820	0.064636	0.061559	0.058587
18.5	0.086395	0.082693	0.079088	0.075582	0.072177	0.068873	0.065673	0.062578	0.059586	0.056698
19.0	0.083839	0.080232	0.076720	0.073305	0.069989	0.066774	0.063659	0.060646	0.057735	0.054926
19.5	0.081430	0.077913	0.074490	0.071162	0.067931	0.064798	0.061764	0.058831	0.055996	0.053262
20.0	0.079155	0.075725	0.072386	0.069140	0.065990	0.062936	0.059979	0.057120	0.054359	0.051695
20.5	0.077004	0.073656	0.070397	0.067230	0.064157	0.061178	0.058295	0.055507	0.052815	0.050218
21.0	0.074967	0.071697	0.068515	0.065423	0.062423	0.059516	0.056702	0.053982	0.051356	0.048823
21.5	0.073035	0.069840	0.066731	0.063711	0.060781	0.057941	0.055194	0.052539	0.049975	0.047504
22.0	0.071200	0.068076	0.065037	0.062086	0.059222	0.056448	0.053764	0.051171	0.048667	0.046254
22.5	0.069455	0.066399	0.063428	0.060541	0.057742	0.055030	0.052406	0.049872	0.047425	0.045068
23.0	0.067794	0.064803	0.061896	0.059072	0.056333	0.053681	0.051116	0.048637	0.046246	0.043941
23.5	0.066210	0.063282	0.060436	0.057672	0.054992	0.052397	0.049887	0.047462	0.045123	0.042869
24.0	0.064698	0.061831	0.059043	0.056337	0.053713	0.051173	0.048716	0.046343	0.044054	0.041848
24.5	0.063254	0.060444	0.057714	0.055062	0.052492	0.050004	0.047598	0.045275	0.043034	0.040875
25.0	0.061873	0.059119	0.056442	0.053844	0.051326	0.048888	0.046531	0.044255	0.042060	0.039946
25.5	0.060551	0.057850	0.055226	0.052679	0.050210	0.047821	0.045511	0.043281	0.041130	0.039058
26.0	0.059284	0.056635	0.054061	0.051563	0.049142	0.046799	0.044534	0.042348	0.040240	0.038209
26.5	0.058069	0.055469	0.052944	0.050493	0.048118	0.045820	0.043598	0.041454	0.039387	0.037396
27.0	0.056903	0.054351	0.051872	0.049466	0.047136	0.044880	0.042701	0.040598	0.038570	0.036617
27.5	0.055783	0.053277	0.050842	0.048481	0.046193	0.043979	0.041840	0.039776	0.037786	0.035870
28.0	0.054706	0.052244	0.049853	0.047533	0.045287	0.043113	0.041013	0.038986	0.037033	0.035152
28.5	0.053669	0.051250	0.048901	0.046623	0.044416	0.042281	0.040218	0.038228	0.036309	0.034463
29.0	0.052671	0.050294	0.047985	0.045746	0.043577	0.041480	0.039453	0.037498	0.035613	0.033800
29.5	0.051710	0.049372	0.047103	0.044901	0.042770	0.040708	0.038717	0.036795	0.034944	0.033162
30.0	0.050783	0.048484	0.046252	0.044088	0.041992	0.039965	0.038007	0.036119	0.034299	0.032547

An approximate correction for the effect of thermal expansion can be made through the formula [*Barron et al.*, 1959]

$$\theta_{cal}(V_0)/\theta_{cal}(V_T) = (\rho_0/\rho_T)^\gamma \qquad (31)$$

where ρ_0 and ρ_T are the densities of the crystal at 0° and T°K and γ is the thermal Grüneisen parameter. Using this formula, *Barron et al.* [1959] have shown that the effect is very small for MgO, being 0.5% at 270°K. The effect is expected to be of similar magnitude for most of the minerals considered here and hence is neglected.

The model gives the contribution of the harmonic lattice vibrations to C_V: Schottky anomalies, electronic or magnetic contributions, defect, domain, or surface contributions, and anharmonic effects have been ignored. Their contribution to the heat capacity is expected to be small except possibly at very low (<10°K) or very high (>500°–1000°K) temperatures. *Gopal* [1966] reviews most of these effects; *Barron et al.* [1959] discuss the effect of anharmonicity and surface contributions for MgO; *Leibfried and Ludwig* [1961] discuss anharmonicity in detail. Anharmonicity is probably the most important of the effects ignored because it becomes noticeable at high temperatures of interest to geologists and geophysicists. For several minerals there is a tendency for $\theta_{cal}(T)$ at high temperatures to decrease with increasing temperature (see Figures 2–4). The same behavior has been observed for some of the alkali halides and interpreted as an anharmonic effect [*Barron et al.*, 1959] because the 'harmonic' contribution to the heat capacity would be expected to give constant $\theta_{cal}(T)$ at these temperatures.

As was mentioned above, the effect of thermal expansion alone would be to cause the spectral frequencies to decrease as the temperature increases. Thus $\theta_{cal}(\infty)$, which would approach a constant value for a harmonic spectrum, would decrease if thermal expansion alone were considered. *Barron et*

al. [1959] have calculated the magnitude of this effect for a number of halides (including sodium chloride) which have low Debye temperatures. Although the expansion does cause a decrease in $\theta_{cal}(\infty)$, it cannot fully explain the magnitudes of the observed decreases in $\theta_{cal}(\infty)$ for the halides. *Barron et al.* [1959] attribute the excess decrease to an increase in heat capacity due to anharmonicity of the lattice vibrations themselves. At high temperatures the mean amplitude of atomic vibrations becomes large in comparison to the interatomic distances, and cubic and quartic terms in the atomic potential (neglected in the harmonic theory) become important. These cubic and quartic terms may give rise to positive and negative contributions, respectively, to the anharmonic heat capacity. The balancing of these two terms depends on details of the interatomic forces.

C_V, calculated from (29) and (30), and $\theta_{cal}(T)$ obtained from these data are shown as dots in Figures 2–4 for the minerals considered here. Data were obtained from references listed in the caption of Figure 4 in paper 1.

5. Temperature Dependence of the Heat Capacity

The temperature dependence of the heat capacity of a number of simple substances and framework silicates is examined in this paper in order to illustrate the effect of composition and structure on the vibrational and thermodynamic properties. Halite, periclase, brucite, corundum, and spinel are considered as examples of simple substances with varying degrees of anisotropy and complexity; the five silica polymorphs, quartz, cristobalite, glass, coesite, and stishovite, are examined as isochemical polymorphs with structural variations; rutile is considered as an anisotropic material and as an analogue of stishovite; and albite and microcline are considered as two typical feldspars. Data used in the model are given in Tables 4 and 5.

The results of the calculations of C_V with the model are given in Figures 2*a*, 3*a*, and 4*a*, where they are compared with experimental data. Curves of $\theta_{cal}(T)$, which are a more sensitive indicator of deviations from the measured values than are the specific heat curves and which clearly show systematic deviations of the model from the data, are shown in Figures 2*b*, 3*b*, and 4*b*. Discrepancies between the model and the data below 100°K are strongly emphasized by the $\theta_{cal}(T)$ curves. The relative contributions of the acoustic, optic continuum and intramolecular modes are given in Figures 2*c*, 3*c*, and 4*c*. The model frequency distributions are shown in Figures 2*d*, 3*d*, and 4*d*, where they are compared with spectral data. Because the complete frequency distribution $g(\nu)$ is not available for most minerals, only infrared and/or Raman data can be

TABLE 3. Einstein Function (24)

x_E	$E(x_E)$	x_E	$E(x_E)$	x_E	$E(x_E)$	x_E	$E(x_E)$
0.1	0.999161	5.1	0.160528	10.1	0.004191	15.1	0.000063
0.2	0.996670	5.2	0.150827	10.2	0.003867	15.2	0.000058
0.3	0.992535	5.3	0.141624	10.3	0.003568	15.3	0.000053
0.4	0.986771	5.4	0.132901	10.4	0.003292	15.4	0.000049
0.5	0.979424	5.5	0.124641	10.5	0.003036	15.5	0.000045
0.6	0.970532	5.6	0.116827	10.6	0.002800	15.6	0.000041
0.7	0.960148	5.7	0.109442	10.7	0.002581	15.7	0.000037
0.8	0.948331	5.8	0.102466	10.8	0.002379	15.8	0.000034
0.9	0.935148	5.9	0.095885	10.9	0.002193	15.9	0.000031
1.0	0.920674	6.0	0.089679	11.0	0.002021	16.0	0.000029
1.1	0.904985	6.1	0.083833	11.1	0.001862	16.1	0.000026
1.2	0.888170	6.2	0.078329	11.2	0.001715	16.2	0.000024
1.3	0.870314	6.3	0.073151	11.3	0.001580	16.3	0.000022
1.4	0.851508	6.4	0.068284	11.4	0.001455	16.4	0.000020
1.5	0.831848	6.5	0.063712	11.5	0.001340	16.5	0.000019
1.6	0.811429	6.6	0.059419	11.6	0.001233	16.6	0.000017
1.7	0.790345	6.7	0.055392	11.7	0.001135	16.7	0.000016
1.8	0.768693	6.8	0.051616	11.8	0.001045	16.8	0.000014
1.9	0.746567	6.9	0.048078	11.9	0.000962	16.9	0.000013
2.0	0.724061	7.0	0.044764	12.0	0.000885	17.0	0.000012
2.1	0.701266	7.1	0.041662	12.1	0.000814	17.1	0.000011
2.2	0.678268	7.2	0.038761	12.2	0.000749	17.2	0.000010
2.3	0.655154	7.3	0.036048	12.3	0.000689	17.3	0.000009
2.4	0.632002	7.4	0.033513	12.4	0.000633	17.4	0.000008
2.5	0.608890	7.5	0.031145	12.5	0.000582	17.5	0.000008
2.6	0.585890	7.6	0.028935	12.6	0.000535	17.6	0.000007
2.7	0.563067	7.7	0.026872	12.7	0.000492	17.7	0.000006
2.8	0.540486	7.8	0.024949	12.8	0.000452	17.8	0.000006
2.9	0.518203	7.9	0.023155	12.9	0.000416	17.9	0.000005
3.0	0.496269	8.0	0.021484	13.0	0.000382	18.0	0.000005
3.1	0.474732	8.1	0.019927	13.1	0.000351	18.1	0.000005
3.2	0.453633	8.2	0.018478	13.2	0.000322	18.2	0.000004
3.3	0.433010	8.3	0.017129	13.3	0.000296	18.3	0.000004
3.4	0.412894	8.4	0.015874	13.4	0.000272	18.4	0.000003
3.5	0.393313	8.5	0.014707	13.5	0.000250	18.5	0.000003
3.6	0.374290	8.6	0.013621	13.6	0.000229	18.6	0.000003
3.7	0.355843	8.7	0.012613	13.7	0.000211	18.7	0.000003
3.8	0.337987	8.8	0.011676	13.8	0.000193	18.8	0.000002
3.9	0.320732	8.9	0.010806	13.9	0.000178	18.9	0.000002
4.0	0.304087	9.0	0.009999	14.0	0.000163	19.0	0.000002
4.1	0.288055	9.1	0.009249	14.1	0.000150	19.1	0.000002
4.2	0.272637	9.2	0.008554	14.2	0.000137	19.2	0.000002
4.3	0.257832	9.3	0.007909	14.3	0.000126	19.3	0.000002
4.4	0.243635	9.4	0.007311	14.4	0.000116	19.4	0.000001
4.5	0.230040	9.5	0.006756	14.5	0.000106	19.5	0.000001
4.6	0.217038	9.6	0.006243	14.6	0.000097	19.6	0.000001
4.7	0.204620	9.7	0.005767	14.7	0.000089	19.7	0.000001
4.8	0.192773	9.8	0.005326	14.8	0.000082	19.8	0.000001
4.9	0.181485	9.9	0.004918	14.9	0.000075	19.9	0.000001
5.0	0.170742	10.0	0.004540	15.0	0.000069	20.0	0.000001

TABLE 4. Data for Acoustic Branches: Simple Minerals and Framework Silicates

Mineral	Commonly Designated Crystallographic Structure	Z (Primitive Cell)	n	$V_{\text{unit cell}}$ ($= V_L$), 10^{-24} cm^3	ρ, g cm^{-3}	u_1, km s^{-1}	u_2, km s^{-1}	$v_{VRH,S}$ km s^{-1}	$v_{VRH,P}$ km s^{-1}	v_m, km s^{-1}	θ_{el}, °K	w_1, cm^{-1}	w_2, cm^{-1}	w_3, cm^{-1}
Halite	fcc[a]	1	2	45	2.16	2.50[b]	2.74	2.61	4.56	2.90	306	93	102	170
Periclase	fcc[a]	1	2	19	3.58	5.83[b]	6.30	6.05	9.71	6.66	942	289	312	482
Brucite	trig	1	5	64	2.37	4.25[c]	4.25	(4.25)	7.36	4.72	697	141	141	244
Corundum	rhom (hex)[a]	2	5	85	3.99	6.12[b]	6.59	6.41	10.85	7.03	1026	184	198	327
Spinel	fcc[a]	2	7	132	3.58	5.31[b]	6.00	5.62	9.82	6.24	879	138	156	255
α-Quartz	trig	3	3	113	2.65	3.76[b]	4.46	4.05	6.05	4.42	567	103	122	165
α-Cristobalite	tetr	4	3	171	2.32	(3.56)[d]	(4.23)	(3.84)	(6.17)	4.23	519	85	101	147
Silica glass	see text	see text	see text	see text	2.20	3.74	3.74	3.74	5.50	4.08	491	see text	see text	see text
Coesite	mono[a]	8	3	274	2.92	4.17[b]	5.24	4.59	8.19	5.10	676	85	107	167
Stishovite	tetr	2	3	47	4.20	(5.05)[e]	(6.16)	(5.50)	11.00	6.16	921	186	227	405
Rutile	tetr	2	3	62	4.26	4.73[b]	5.73	5.14	9.26	5.72	781	158	191	309
Albite	tri	4	13	665	2.62	2.98[b]	3.91	3.33	6.06	3.70	472	45	59	92
Microcline	tri	4	13	722	2.56	3.02[b]	3.85	3.34	6.02	3.72	460	45	57	89

[a]For these substances the primitive cell differs from the commonly designated crystallographic cell.
[b]References for data given in Table A1 of paper 1.
[c]Anisotropy not included because of lack of data (see text).
[d]Assumed $v_{VRH,S}/\rho = 1.62$; $v_{VRH,P}/\rho = 2.65$ [after *Anderson and Liebermann*, 1966]. Assumed $u_2/v_{VRH,S} = 1.10$, as for quartz.
[e]Values of v_{VRH} from *Mizutani et al.* [1972]; assumed $u_2/v_{VRH,S} = 1.12$, as for rutile.

shown for many minerals. It should be remembered that the frequency distribution inferred from such spectroscopic data taken at $\mathbf{K} = \mathbf{0}$ is incomplete because dispersion curves are not known over the whole Brillouin zone.

In all cases the heat capacities given by the model developed here are in much better agreement with the measured heat capacities than are heat capacities calculated from the Debye model with θ_D based on θ_{el}. (Such a model would give straight lines at the 0°K value of $\theta_{cal}(T)$ marked by an asterisk in the curves of Figures 2*b*, 3*b*, and 4*b*.) For simple substances (halite, periclase, spinel, and corundum) the heat capacity predicted by the model exhibits nearly Debyelike behavior in that $\theta_{cal}(T)$ attains a constant value at relatively low temperatures. The heat capacity of the more complex substances is not at all Debyelike. For these substances the single-parameter Debye model is quite inadequate to predict the specific heat. This conclusion holds even if the Debye temperature is chosen arbitrarily as a free parameter, for example, to match an observed heat capacity at 298°K. The only temperature range where a single-parameter Debye model might be used with confidence is at high temperatures where $\theta_{cal}(\infty)$ is approached. In this region a Debye (or an Einstein) model with θ_D (or θ_E) equal to $\theta_{cal}(\infty)$ might be appropriate.

Halite and Periclase

Halite (NaCl) and periclase (MgO) (see Figure 2) have one formula unit in the fundamental Bravais unit cell. They thus have six vibrational modes, three of which are acoustic. The mode partitioning obtained from models which choose a primitive unit cell as the fundamental vibrating unit is very different from the mode partitioning obtained from models which choose other vibrating units; for example, *Raman* [1943, 1961] postulated a supercell for NaCl which contained 16 particles, eight cations and eight anions. According to his

TABLE 5. Data for Optical Spectra of Simple Minerals and Framework Silicates

Mineral	$w_t(\mathbf{0})$, cm^{-1}	$w_t(\mathbf{K}_{max})$, cm^{-1}	w_u, cm^{-1}	w_E, cm^{-1}	q	Comments
Halite	173	135	265			
Periclase	390	303	730			
Brucite	280	198	725	3670	0.13	
Corundum	378	300	751			
Spinel	225	178	600	700	0.22	model 1
	225	178	750			model 2
α-Quartz	128	91	809	1100	0.22	
α-Cristobalite	see text	84	804	1100	0.22	
Silica glass	see text	5	804	1100	0.22	model 1 (CRN)
	see text	14	805	1100	0.22	model 2 (PD)
Coesite	121	86	683	1100	0.22	model 1
	121	86	792	1100	0.22	model 2
Stishovite	330	233	950			model 1
	330	233	769	920	0.22	model 2
Rutile	113	80	840			model 1
	113	80	500	610	0.05	model 2
				824	0.17	
Albite	83	63	648	1000	0.21	
Microcline	74	62	648	1000	0.21	

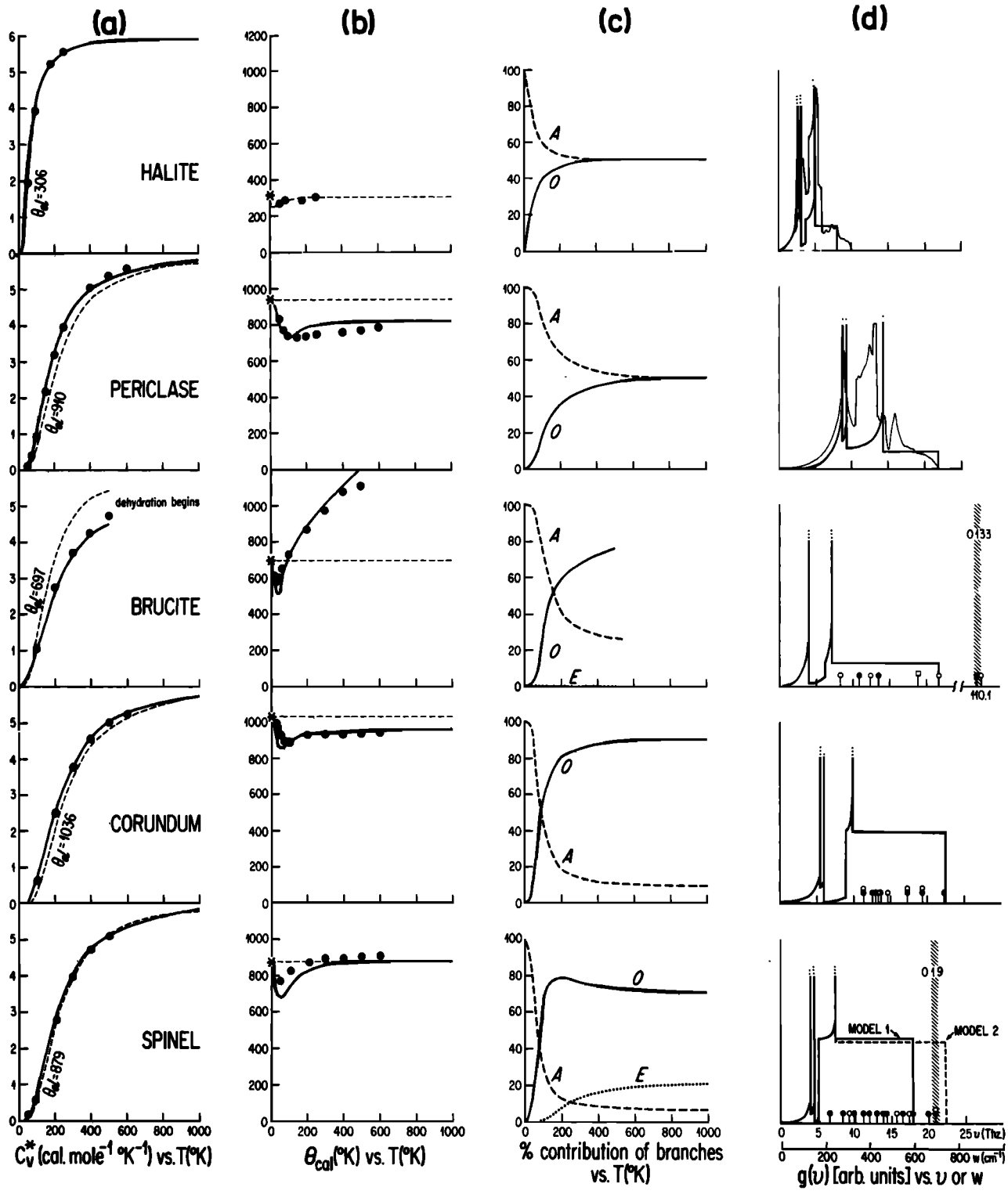

Fig. 2. Data and model values for halite, periclase, brucite, corundum, and spinel. (*a*) Heat capacities as a function of temperature. (*b*) Calorimetric Debye temperatures as a function of temperature. (*c*) Percent contribution to heat capacity of acoustic modes *A*, optic continuum *O*, and Einstein oscillator *E* as a function of temperature. (*d*) Model spectra compared to lattice dynamics calculations (for NaCl) or Raman (solid circles), infrared (open circles), or INS (squares) data. The vertical scale shown on spectra in Figures 2, 3, and 4 is arbitrary. Frequencies are given as ν (terahertz) and w (cm^{-1}). The singularities in the acoustic branches at ν_1, ν_2, and ν_3 are indicated by three dots on the acoustic branches. Parameters used in the model are given in Tables 4 and 5. References to heat capacity data are given in Figure 4 of paper 1. References to spectral data are given in paper 2.

model, acoustic modes account for only $3/(3 \times 16) = \frac{1}{16}$ of the degrees of freedom, 'a small residue' of the total modes [*Raman*, 1943, p. 250], in contrast to the 50% consistent with the choice of the Bravais cell as the fundamental vibrating unit.

Because the atoms in both halite and periclase are rather homogeneously bonded, the wave velocities of these substances are nearly isotropic, although periclase exhibits considerably more anisotropy than halite. The shape of acoustic branches given by the assumed sine wave dispersion law agrees well with the form of measured dispersion curves (see paper 2, Figure 5) because the substances are nearly 'monatomic' in the sense of the criteria 1–4 in section 3 of paper 1.

The optic modes of halite span a relatively small range of frequencies (173–256 cm^{-1} at $\mathbf{K} = 0$). There are only three optic modes (see Figure 2*a* of paper 2). The modes show some dispersion through the Brillouin zone (particularly the longitudinal optic mode, which dips as low as 180 cm^{-1} at $K = 1.414(2\pi/a)$ in the [110] direction [*Raunio et al.*, 1969, p. 1497]. The simple dispersion relation adopted for the lowest TO optic branch in the model ($\omega(\mathbf{K}_{max}) = \omega(0)/(1 + m_2/m_1)^{1/2}$, where m_2 is the mass of sodium and m_1 the mass of chlorine) predicts a value of 135 cm^{-1} for the TO branch at the zone edge, in reasonable agreement with the observed value of 142 cm^{-1} (at $\mathbf{K} = 0.5(3^{1/2})(2\pi/a)$ in the [111] direction).

The optic modes of periclase lie at higher frequencies than those of halite because the Mg-O force constants are greater than the Na-Cl force constants and the atoms are less massive. The LO and TO modes are relatively widely spaced at $\mathbf{K} = 0$: the LO mode is at 730 cm^{-1} and the TO mode is at 390 cm^{-1}. As can be seen from measured dispersion curves (Figure 2*b* of paper 2) the zone center frequency of the LO branch is a maximum for the branch, and the frequency for the TO branch is a minimum for the branch. In the model the optic modes were represented by a continuum extending from 303 to 730 cm^{-1}; the value 303 cm^{-1} was obtained by the correction of the $\mathbf{K} = 0$ value of 390 cm^{-1} for dispersion across the Brillouin zone by the factor $(1 + m_2/m_1)^{-1/2}$, where m_2 is the mass of oxygen and m_1 is the mass of magnesium.

The model vibrational spectra for these two substances are shown in Figure 2*d*, where they are compared with spectra obtained from detailed lattice vibrational calculations. The vertical scale in these figures is arbitrary and is not the same for the various spectra; therefore only positions and relative magnitudes of features can be compared. Although the model spectra have an 'artificial' appearance arising from the sharpness of the three acoustic modes (which have singularities at ν_1, and ν_2, and ν_3, shown schematically by dotted extensions of the modes) and from the arbitrariness of the flat continuum, they are useful in showing the major features of the vibrational spectra. They show good qualitative agreement with the more detailed spectra obtained from lattice dynamics calculations: the extent of the acoustic modes is approximately correct, as are the peaks in the spectra due to these modes; the overlap of acoustic and optic modes at low frequency is correct for halite, and the relative proportions of acoustic and optic modes are correct. The agreement is not as good for periclase because the model spectrum includes too many oscillators at high frequencies (near the $\mathbf{K} = 0$ longitudinal optic mode).

The heat capacity of halite is predicted well by the model spectrum; that of periclase is predicted slightly less accurately. The 10° drop in $\theta_{cal}(T)$ at low temperature for halite and the much larger decrease (80°K) in $\theta_{cal}(T)$ for periclase match measured data. From examination of the relative contributions of acoustic and optic modes to the heat capacity (Figure 2*c*) it can be seen that these decreases are caused mainly by anisotropy and dispersion in the acoustic branches. The subsequent small recovery of the $\theta_{cal}(T)$ curves toward $\theta_{cal}(0)$ is due to the increasing contribution of the optic modes as the temperature increases.

The deviation of the periclase model heat capacity from measured data above 200°K arises from the use of the $\mathbf{K} = 0$ value of 730 cm^{-1} for the upper limit of the optic continuum. For this mode the $\mathbf{K} = 0$ value is a maximum and the frequency decreases substantially (to ~500 cm^{-1} at the zone boundary in the [001] direction). Because the modes near the zone center are more heavily weighted in the calculation of the vibrational spectrum, the zone center value of the mode frequency does not accurately represent the average frequency of the mode across the Brillouin zone. As can be seen from the actual vibrational spectrum shown in Figure 2*d*, a value of 500–600 cm^{-1} would be more representative of the directionally averaged value of the LO mode; use of this value in the model gives heat capacities in excellent agreement with measured values. Although many modes show a similar decrease from a maximum value of frequency at the zone center to a lower value at the zone edge, some modes show the opposite behavior (see the dispersion relations in Figures 2*a*–2*e* of paper 2). The degree of dispersion and its trend depend on the interatomic forces, and it is not possible to specify a priori a simple dispersion curve for the high-frequency optic modes. To the extent that the modes decrease in frequency toward the zone edge, the model, with vibrational frequencies chosen from optical data alone, will tend to give low estimates of C_V (as occurs in the case of periclase) because the average frequencies of the optic branches will be somewhat lower than those specified in the model. A similar problem would be encountered in the 'spectroscopic model' described above, in which each optic mode was represented by an Einstein oscillator placed at the $\mathbf{K} = 0$ frequency of the mode; dispersion is not accounted for in such a model.

Brucite

Brucite ($Mg(OH)_2$) has one formula unit in the fundamental Bravais unit cell: it therefore has 15 vibrational modes per unit cell, three of which are acoustic. The addition of a formula unit of H_2O to form brucite from periclase results in an increase of the total number of degrees of freedom for the unit cell from six to 15 and a reduction of the fraction of acoustic modes from 50% to 20%.

The only acoustic velocity data available for brucite are shock wave data [*Simakov et al.*, 1974] which give a sound velocity (interpreted to be a bulk sound speed) of 4.75 km s^{-1} (corresponding to an elastic Debye temperature of 697°K). A value of Poisson's ratio of 0.25 was used to estimate v_S and v_P from this bulk sound speed. Although the structure of brucite is highly anisotropic, viz., cleavage, acoustic anisotropy could not be reliably included in the model because of the uncertainty in the acoustic data. The acoustic branches calculated from these wave velocities peak at 141 and 244 cm^{-1} at the Brillouin zone boundary. Inelastic neutron scattering data show an acoustic mode at 128 cm^{-1} [*Safford et al.*, 1963; *Pelah et al.*, 1965] which may correspond to the top of the slow acoustic shear branch.

At $\mathbf{K} = 0$ the optic modes of brucite (280–725 cm^{-1}) lie relatively close to those of periclase (390–730 cm^{-1}) except for the O-H stretching modes, which are at 3700 and 3655 cm^{-1}. When it is corrected by the factor $(1 + m_2/m_1)^{-1/2}$ (where m_1 is the mass of magnesium and m_2 is the mass of oxygen), the zone

center frequency of the lowest mode (280 cm^{-1}) becomes 215 cm^{-1} at the zone boundary. The optic continuum was therefore taken from 215 to 725 cm^{-1}. The O-H modes were approximated as a single Einstein oscillator at 3670 cm^{-1} containing 13.3% of the total modes. The model vibrational spectrum is shown in Figure 2*d*.

The heat capacity of brucite to 500°K is shown in Figure 2*a*. Above 500°K, dehydration begins, and the measured heat capacity begins increasing rapidly owing to the onset of the dehydration reaction [*Freund and Sperling*, 1972]. (It should be noted here that C_p data given by Freund and Sperling are approximately 30% lower than the data of *Giauque and Archibald* [1937] used in the figure. No explanation can be given for the discrepancy.) The heat capacity is predicted well by the model at low temperatures. The low-temperature decrease in $\theta_{cal}(T)$ arises from the acoustic shear and longitudinal branches. Optic modes do not contribute appreciably to C_V until temperatures reach ~100°K. The O-H stretching modes do not contribute to C_V at temperatures below those at which dehydration begins.

Corundum

The Bravais unit cell of corundum (Al_2O_3) contains two formula units of Al_2O_3 and therefore has 30 degrees of freedom, 10% of which belong to acoustic modes. Anisotropy was included in the acoustic velocities for the shear branches, but it is minor.

Numerous papers have been published on the optical vibrational modes of corundum. Well-documented infrared-active modes exist at 635, 583, 569, 442, 400, and 385 cm^{-1}, and well-documented Raman-active modes at 751, 645, 578, 451, 432, 418, and 378 cm^{-1} (see Table 1 of paper 2). Inelastic neutron scattering (INS) data do not exist. It is of interest that the modes of corundum do not extend to nearly as low frequencies as the modes of spinel ($MgAl_2O_4$), perhaps an indication that the lowest-frequency modes in spinel are not simply Al-O deformational modes. For the model it was assumed that the zone center frequency of the lowest mode in the optic continuum was 378 cm^{-1}, which was reduced to 300 cm^{-1} at the zone boundary by correction for dispersion across the Brillouin zone (with m_2 taken as the mass of oxygen and m_1 as the mass of aluminum). The calculated spectrum for the model is shown in Figure 2*d*, where it is compared with IR and Raman data.

The heat capacity of corundum (shown in Figure 2*a*) is nearly Debyelike. There is a small decrease in $\theta_{cal}(T)$ at 50°–100°K caused primarily by dispersion in the acoustic shear branches. The shear branches contribute to C_V in excess of the Debye behavior predicted from a mean sound speed. The excess is offset, however, by relatively high frequencies for the longitudinal acoustic branch and for the optic continuum. By 300°K, $\theta_{cal}(T)$ rises back to a value only slightly lower than θ_{el}; hence the room temperature specific heat would be well predicted by a θ_{el} based on elastic constants even though C_V at room temperature is actually determined primarily by the optic modes (see the relative contributions in Figure 2*c*). The high-temperature value of $\theta_{cal}(T)$ of ~900°K is characteristic of minerals with Al-O stretching modes as the highest frequency modes.

A comparison of the model heat capacities with measured values near 50°K suggests that dispersion in the acoustic branches is overestimated by the assumed sinusoidal dispersion curves (equation (11)). This is an example of how the heat capacity model developed here may actually be used to suggest features of the vibrational spectrum, namely, that the acoustic modes are less dispersed than the sinusoidal dispersion law suggests and, in particular, that shear modes may extend to frequencies higher than the 184 and 198 cm^{-1} predicted by such a law. A rough estimate suggests that these modes may be near 230 cm^{-1}.

Spinel

Normal spinel ($MgAl_2O_4$) is cubic with two formula units (14 atoms) in the unit cell. The oxygen atoms are approximately in cubic close packing. The magnesium atoms are in positions of fourfold coordination within a tetrahedral group of oxygen atoms; the aluminum atoms are in sixfold coordination within an octahedral group [*Bragg et al.*, 1965, p. 103]. There are 42 degrees of freedom per unit cell, 3 of which (7%) are acoustic.

Like halite and periclase, spinel exhibits relatively little acoustic anistropy because of its cubic symmetry. The shear velocities used are 5.31 and 6.00 km s^{-1}; the compressional velocity is 9.82 km s^{-1}. The mean velocity is 6.24 km s^{-1}, and the acoustic Debye temperature θ_{el} is 879°K.

The optic modes extend from 225 cm^{-1} (Raman active) to 750 cm^{-1} (Raman and infrared active); a weak mode at 825 cm^{-1} reported by *Fraas and Moore* [1972] is ignored here because it is probably related to sample inpurities. It is interesting that although the highest-frequency bands of spinel are at exactly the same wave numbers as those of corundum, they are not attributed to Al-O deformations but to Mg-O vibrations [*Preudhomme and Tarte*, 1971*a*, *b*, *c*, 1972]. These vibrations are reasonably well isolated from the rest of the bands which lie below 600 cm^{-1}. Accordingly, they are modeled by an Einstein oscillator at 700 cm^{-1} containing 19% of the total modes (see paper 2, Table 6). For comparison a second model is shown in which these modes are included as part of the optic continuum. The lowest observed mode at 225 cm^{-1} is lowered to 178 cm^{-1} at the Brillouin zone boundary by the assumed dispersion relation. The model vibrational spectrum for spinel is shown in Figure 2*d*, where it is compared with IR and Raman data. It should be noted that the spectrum is significantly different from the periclase and corundum spectra at low frequencies and thus cannot be modeled as the simple 'sum' of these two spectra. (This raises the interesting question of whether calorimetric properties of spinel can be calculated as the simple sum of the component oxides, periclase and corundum.) The model spectrum also shows clearly that in contrast to the simpler substances such as periclase the acoustic modes comprise only a small fraction of the total modes for spinel.

The heat capacity C_V^* and $\theta_{cal}(T)$ predicted by the model for spinel are given in Figures 2*a* and 2*b*. The properties are similar to those of corundum except at low temperatures where $\theta_{cal}(T)$ approaches a much lower value of θ_{el}. The heat capacity is overestimated by the model in the low-temperature range. Below 80°K the main contribution to the heat capacity is from the acoustic modes, and therefore the excess heat capacity predicted by the model is probably due to an overestimate of the amount of dispersion in these modes. The low-frequency optic modes contribute significantly to the heat capacity above 80°K, and the excess heat capacity of the model in this range must therefore be attributed to an excess of oscillators in the low-frequency part of the optic continuum. At high temperature the heat capacity of spinel is slightly larger than that of corundum. This is most easily seen by comparison of the $\theta_{cal}(T)$ curves: $\theta_{cal}(\infty)$ is ~960°K for corundum and ~875°K for spinel. This might initially be unex-

pected because the highest-frequency modes for both substances are at 750 cm^{-1}. A comparison of the model vibrational spectra in Figure 2*d* reveals the cause of this behavior: the optic continuum of spinel extends to lower wave numbers (178 cm^{-1} at the zone boundary) than that of corundum (300 cm^{-1} at the zone boundary), and because of this extension of the optic continuum to low frequencies, there are relatively fewer oscillators at high frequencies for spinel. It was demonstrated in paper 1 that not only is the frequency of the highest-frequency modes important in determining the high-temperature behavior, but also the relative proportion of the total modes at high frequency. In this case a smaller proportion of the modes are at high frequency for spinel than for corundum.

Quartz, Cristobalite, Glass, and Coesite

These SiO_2 polymorphs with fourfold coordination provide a test of the sensitivity of the model to structural variations and an opportunity to examine the extension of the model to amorphous substances. The most important structural parameters which vary are the unit cell volumes and the number of atoms in the unit cell. Variations in the acoustic velocities and in the degree of anisotropy cause minor variations in the heat capacity.

Structure of SiO_2 polymorphs. The structures of the crystalline silica polymorphs are well known [e.g., *Sosman*, 1965] and will not be reviewed here. The crystalline phases—quartz, cristobalite, and coesite—have 27, 36, and 72 degrees of freedom, respectively, per unit cell. The three acoustic modes therefore comprise 11% of the total modes for quartz, 8.3% for cristobalite, and 4.2% for coesite.

The detailed structure of silica glass, however, is not well known and has been the subject of much controversy [*Gaskell*, 1970; *Bell et al.*, 1968; *Bell and Dean*, 1970; *Wong and Whalley*, 1970]. Except at very low temperatures and frequencies, the heat capacity and Raman and infrared spectra are sufficiently similar to those same properties of quartz and cristobalite to suggest that certain aspects of lattice vibrational theory as developed for crystalline materials apply also to the vitreous state. Vibrational models based on the choice of the SiO_4^{-4} tetrahedron as the fundamental vibrating unit have been successful in accounting for those features of the vibrational spectrum which occur above wave numbers of several hundred cm^{-1} [*Gaskell*, 1970; *Bell et al.*, 1968; *Bell and Dean*, 1970]. The work of *Bell et al.* [1968] and *Bell and Dean* [1970] and the experiments of *Leadbetter* [1969], however, suggest that although it may be theoretically possible to describe the higher-frequency vibrations in glasses by considering structural units similar to the crystalline analogues, it is unlikely that the behavior of the low-frequency branches will be similarly modeled.

The two theories of glass structure which satisfy most existing data (X ray, transmission electron microscope, spectral, and thermodynamic) differ substantially in their description of long-range order in glasses. These theories are referred to as the 'continuous random network' (CRN) theory and the 'paracrystalline' or 'microcrystalline' theory. In both theories the basic structural unit is accepted to be the XY_4 tetrahedron (e.g., SiO_4^{-4}), and adjacent tetrahedra are linked by common Y atoms into a three-dimensional network. The nature of the bridging bonds between tetrahedra is the subject of the controversy.

The continuous random network theory, first developed by *Zacharaisen* [1932, 1935] proposes that vitreous materials are made up of extended three-dimensional networks which lack periodicity at any scale. Modern CRN theories (e.g., *Evans and King*, 1966; *Bell and Dean*, 1966] are special cases of the Bernal theory of the structure of liquids, a theory for the random packing of monatomic spheres. CRN theories require that the structure be essentially irregular throughout the crystal. The randomness of structure in a silica glass is attributed to randomness in the Si-O-Si angles and in the rotation of adjacent tetrahedra about the connecting Si-O bonds. CRN theory holds that there is a definite difference between the vitreous state and the crystalline state, not a gradational change in structural properties between the two states.

The original microcrystalline theory for glass structure predates the Zacharaisen CRN theory by several years [*Randall et al.*, 1930]. The original suggestion was that individual unit cells of cristobalite (having dimensions on the order of 7 Å) were present in glass. The first systematic X ray investigations of glasses [*Warren*, 1933, 1934, 1937; *Warren and Biscoe*, 1938] demonstrated that the presence of such cells was incompatible with X ray data. Hence the original microcrystalline theory was discarded in favor of the then newly published Zacharaisen CRN theory.

The modern microcrystalline view, which will be called the paracrystalline theory here, maintains that in glasses, individual molecules, ions, or atoms are assembled into small or large groups which have a high degree of short-range order compared to the long-range order in the glass [*Valenkov and Porai-Koshitz*, 1936]. The structural groups can be regarded as small distorted crystals, separated from one another by zones of less order. In contrast to the CRN theory the paracrystalline theory maintains that there is not a sharp distinction between the glassy and crystalline states.

For purposes of the thermodynamic calculations I examined the consequences of the paracrystalline model of *Robinson* [1965]. In this model it is proposed that vitreous materials are made up of a jumble of n-sided polyhedra, each face of which is a polygon with m sides. Glass is thereby considered to be a grained, textured polycrystalline structure composed of tiny cylinders whose packing fraction is very high. By a series of arguments, Robinson concluded that the polygons are either pentagons or hexagons, that is, $m = 5$ or 6. He chose to examine the structure composed of puckered pentagonal dodecahedra which have 12 faces. The pentagonal dodecahedra have an equivalent radius of 3.91 Å and have five SiO_2 molecules per dodecahedron. Randomness in a glass composed of pentagonal dodecahedra results from a randomness in the O-Si-O angles about the tetrahedral value, some randomness in the Si-O-Si angle, and a randomness in the amount of distortion in the individual polydodecahedra. Submicroscopic structural units of glass, such as those observed in transmission electron microscope (TEM) bright field and dark field micrographs [*Prebus and Michener*, 1954; *Zarzycki and Mezard*, 1962; *Gaskell and Howie*, 1974], were hypothesized by Robinson to be tiny cylinders containing about 225 polydodecahedra (1125 SiO_2 molecules) each. Glass was thus believed by Robinson to be comprised of a grained, textured structure of these cylinders whose packing fraction is very high. The density of the submicroscopic structural units (cylinders) is 2.29 g cm^{-3}, and the 'microporosity' arising from imperfect cylindrical packing of the grains is about 5%.

Neither the CRN nor the paracrystalline model can be treated rigorously by a lattice dynamics model because neither model advocates the existence of a unit cell regularly repeated throughout the glass by translational periodicity. The para-

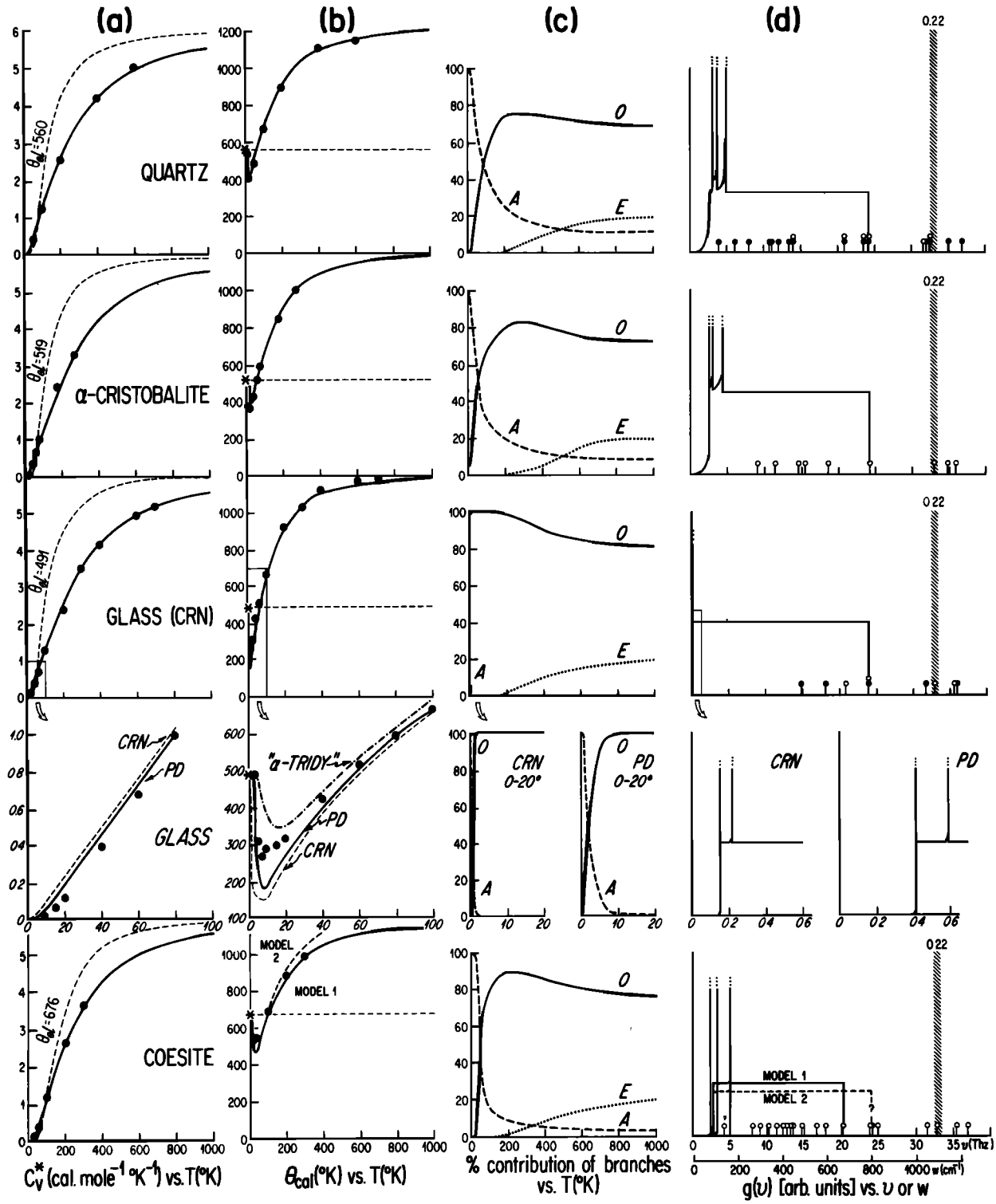

Fig. 3. Data and model values for quartz, cristobalite, glass, and coesite. (*a*) Heat capacities as a function of temperature. (*b*) Calorimetric Debye temperatures as a function of temperature. (*c*) Percent contribution to heat capacity of acoustic modes *A*, optic continuum *O*, and Einstein oscillator *E* as a function of temperature. (*d*) Model spectra compared to optical data or INS data. The notation is the same as that in Figure 2.

crystalline model, however, may be loosely interpreted to specify a structure rather like a unit cell, e.g., the submicroscopic cylindrical units of Robinson, consisting of 1125 SiO_2 molecules in a cylinder of 25 Å diameter and 100 Å length. For this choice of 'pseudo unit cell,' with 1125 SiO_2 molecules per grain, there are 9975 (approximately 10,000) degrees of freedom per cylinder, three of which are acoustic. Although this 0.03% is a very small fraction of the total modes, the contribution of these modes would be measurable at low temperatures, as is shown in Figure 3.

The CRN model does not lend itself to treatment by analogy to the lattice dynamics approach for crystals because of its

basic principle that there is no small repeat unit in amorphous substances. In essense, in this model the structural unit of glass is the macroscopic grain; in a typical heat capacity experiment [e.g., *Flubacher et al.*, 1959] the macroscopic grains are several millimeters in diameter. A description of the lattice vibrations of such a substance can be obtained only by solving the dynamical matrix for the motions of a very large number of atoms (approximately Avogadro's number), those in the macroscopic grain. Current practice is to make physical models of small parts of the CRN structures and to study the modes of vibration of large numbers of atoms in these physical models [e.g., *Evans and King*, 1966; *Bell and Dean*, 1966; *Bell et al.*, 1968]. The three acoustic modes belonging to such particles are a negligible fraction ($<10^{-24}$) of the total degrees of freedom and for all practical purposes do not appear in a vibrational spectrum and do not contribute measurably to the heat capacity. To approximate the CRN model, I have examined a model for glass in which the acoustic modes are 10^{-6} of the total modes; this fraction is picked arbitrarily (as one which the computer program handles easily). The reader should keep in mind that the purpose of examining the heat capacity of the silica polymorphs, including glass, in the context of the model proposed for heat capacities in this paper, is to examine the consequences of structural variations, particularly variations in the size of the unit cell. The treatment of glass as proposed above shows the behavior of the model as the unit cell approaches infinite size.

Additional model data for the SiO_2 polymorphs. The SiO_2 polymorphs are characterized by relatively low wave velocities because of their open structure and generally low densities. Shear velocities range from 3 to 5 km s^{-1}, and compressional velocities vary from 5 to 7 km s^{-1}. Directionally averaged maximum and minimum shear velocities can be estimated for quartz from single-crystal elastic data [*McSkimmin et al.*, 1965]. The slow shear velocity u_1 is estimated to be 3.76 km s^{-1}, and the fast shear velocity u_2 is 4.46 km s^{-1} (see the appendix of paper 1). Slow and fast shear velocities and Voigt-Reuss-Hill (VRH) shear and longitudinal velocities for all of the polymorphs are given in Table 4. The slow and fast shear velocities given for glass, cristobalite, and coesite are estimates (see the appendix of paper 1).

The optic modes of quartz, cristobalite, and glass are remarkably similar at high frequencies. Si-O stretching modes comprise 22% of the total degrees of freedom in each case and occur in an isolated band centered near 1100 cm^{-1}. There is a weak absorption band in the infrared spectrum at 792 cm^{-1} which might correspond to the top of the optic continuum of coesite (Figure 1*a* of paper 2). However, the heat capacity predicted by the model with this band as the top of the optic continuum is a poor fit to measured data, and it will be suggested below that the top of the optic continuum is at 683 cm^{-1}, the next highest observed mode in infrared spectra. In this case the 794-cm^{-1} band might be an impurity band (see the discussion of impurities in coesite in paper 2) or might be one of the stretching modes at anomalously low frequency; results from both cases are given in Figure 3.

The lower cutoff of the optic continuum is well defined only for quartz (ω_l = 128 cm^{-1}). The infrared spectrum of coesite shows a continuous series of optically active lines extending down to 265 cm^{-1}. Raman data are not available. Because the two shear and one longitudinal acoustic branches extend to 85, 107, and 167 cm^{-1}, respectively, it is highly probable that optic modes extend lower than the infrared data suggest. The value ω_l = 121 cm^{-1} was estimated by applying the one-dimensional model for the separation of acoustic and optic modes to the calculated acoustic branches; this cutoff is lowered to 86 cm^{-1} by the dispersion assumed across the Brillouin zone. The lower cutoff is even less well defined for cristobalite and glass, although in both cases, Raman data or INS data are available (see paper 2). Far-infrared spectra obtained in this study (paper 2) do not reveal any distinct absorption bands below 298 cm^{-1} for cristobalite or any bands below 470 cm^{-1} for glass (paper 2). Raman spectra of vitreous silica [*Flubacher et al.*, 1959] show an intense continuum extending continuously from 560 down to 8 cm^{-1}. This continuum was originally attributed by *Flubacher et al.* [1959] to optical modes of very low frequency. Later inelastic neutron scattering work [*Leadbetter*, 1969] attributed the vibrational modes of glass at $w \lesssim$ 40 cm^{-1} to much broadened transverse acoustic branches. Because the neutron scattering differential cross section for fused silica was observed to be almost identical to that for cristobalite for $w > 50$ cm^{-1}, it was suggested that the optic mode distribution may be the same as that of cristobalite above this wave number. The neutron scattering results for both substances suggest that the optic modes merge with and are indistinguishable from the acoustic modes. It will therefore be assumed in this model that the optic continuum of both substances extends down to the lowest acoustic branch at the Brillouin zone boundary, that is, $w_l = w_1$. For cristobalite this means that w_l is at 85 cm^{-1}; for the CRN model glass, w_l is at 5 cm^{-1}, and for the paracrystalline model glass, w_l = 13.5 cm^{-1}.

Results. The heat capacities calculated from the model are shown in Figure 3*a*. The calculated heat capacities for the crystalline polymorphs are in excellent agreement with measured values. In the case of coesite this must be considered fortuitous in view of the assumptions made about the optic continuum. The only significant deviations occur at temperatures below 50°K. Even at very low temperatures (<20°K), where the acoustic branches make the dominant contribution to the heat capacity and where the thermodynamic properties are sensitive to details of the spectrum, the model results are in good agreement with measured data for quartz and coesite. The major discrepancy between the model and the data is in the region of temperatures where the lowest-frequency optic modes make an appreciable to major contribution to the heat capacity (20°–100°K). For coesite the discrepancy is negligible; for quartz and cristobalite the heat capacity is underestimated, as is shown best by the $\theta_{cal}(T)$ curves (Figure 3*b*). Examination of the relative contributions of acoustic and optic branches shows that the model discrepancy arises from both branches: for the acoustic branches, anisotropy may be overestimated, or, more likely dispersion is underestimated (see the discussion of spectra which follows), and for the optic branches, w_l may be overestimated. At temperatures above 100°K the optic continuum makes the major contribution to the heat capacity. The contribution of the Si-O stretching modes is appreciable at room temperature.

The excellent agreement of the model heat capacities with measured heat capacities does not of course imply a similarly detailed match of the model vibrational spectra with measured vibrational spectra. Nevertheless, some of the major important spectral features are included in the model, as may be seen by comparing the measured and calculated spectra shown in the figures. Consider the spectrum of quartz, for which the neutron scattering experiments of *Elcombe* [1967, p. 954] have provided dispersion curves. The acoustic velocities used in the model and the assumed sine wave dispersion give model acoustic branches which are in reasonable agreement with the mea-

sured acoustic dispersion curves found by *Elcombe* [1967, p. 954]. The frequencies at the zone boundary and the assumed sinusoidal shapes are qualitatively correct, but on the average the model appears to underestimate somewhat the amount of dispersion. Elcombe's experimental data for the normal modes in the z direction and *Leadbetter*'s [1969] determination of the spatially averaged dispersion curve place the lowest shear branch in the range 55–80 cm^{-1}, somewhat below the model value of 103 cm^{-1}. The same trends are noted for cristobalite. Inelastic neutron scattering experiments on cristobalite [*Leadbetter*, 1969] indicate truncation of the shear branches at 30–50 cm^{-1} and 60–85 cm^{-1}, substantially below the model values of 85 and 101 cm^{-1}, respectively. Leadbetter comments that the lowest shear branch is highly dispersed and flattens off at remarkably low energy.

Both models discussed for glass predict a heat capacity which is far greater than that of quartz or cristobalite at temperatures of a few degrees Kelvin (see Figure 3*b*), although both models slightly overestimate the amount of excess. This excess heat capacity is well known and appears to be characteristic of amorphous materials in general [e.g., *Anderson*, 1959; *Fritzsche*, 1973, p. 118; *Antoniou and Morrison*, 1965; *Robie et al.*, 1978]. The measured excess heat capacity may be expressed as the sum of two terms with different behavior: a term linear with temperature and a term cubic with temperature and of larger magnitude than is expected from simple Debye theory [*Fritzsche*, 1973]:

$$C_V = AT + BT^3 \tag{32}$$

The specific heat proportional to T^3 arises from a phonon density of states $g(\omega)$ proportional to ω^2; however, the coefficient of proportionality is not that obtained from the elastic constants. The linear term dominates below about 1°K [*Zeller and Pohl*, 1971]; the coefficient A is 10 ergs g^{-1} $°K^2$ to within a factor of 2. The linear term can be derived from a density of states spectrum of phonon excitations which is independent of energy (as is the optic continuum of this paper) with a density of the order of 10^{21} cm^{-3} eV^{-1} between $0 < E < 2 \times 10^{-3}$ eV [*Fritzsche*, 1973, p. 119]. The cause of both excess heat capacity terms has been the subject of much debate in the literature.

Flubacher et al. [1959] and *Leadbetter* [1969] concluded that excess phonon modes at low frequencies were required to explain the low-temperature heat capacity and postulated that these modes arise from two sources: (1) localized modes at $w <$ 20 cm^{-1} and perhaps as low as 6–9 cm^{-1} arising from structural defects such as oxygen vacancies and (2) a mode at about 40 cm^{-1} containing about 1.5% of the total modes. This 40-cm^{-1} mode is also observed in cristobalite, in which it appears to contain 2–3% of the total modes. There is strong evidence that at very low energies ($w < 20$ cm^{-1}) localized modes associated with structural defects such as oxygen vacancies are important. These modes comprise about 1 in 10^4 of the degrees of freedom and account for the linear term in (32) [*Leadbetter*, 1969]. The cause of the excess heat capacity proportional to T^3 has not been so well established. *Smythe et al.* [1953] and *Anderson* [1959] proposed that low-frequency bending of a weak elongated Si-O-Si bond contributed to the excess specific heat. *Anderson and Bömmel* [1955] argued that this mode was the cause of the low-temperature acoustic absorption in vitreous silica. *Clark and Strakna* [1962] showed that the elongated Si-O-Si bond acts as a Schottky type of defect and can explain that part of the excess heat capacity below 30°K. However, the neutron scattering experiments of *Wong and Whalley* [1970] and *Leadbetter* [1969] on various forms of silica and of *Leadbetter and Litchinsky* [1970] on vitreous germania, have led to a different interpretation—that the excess low-frequency mode is a broadened transverse acoustic branch.

In the model of this paper the low-frequency modes are treated formally as optic modes belonging to the optic continuum. This continuum extends down to and is continuous with the acoustic branches; however, the density of state changes abruptly at the optic continuum because for both the continuous random network (CRN) and the pentagonal dodecahedral model (PD) the acoustic modes are a very small fraction of the total modes ($\sim 10^{-6}$ in the computer model for the CRN and $\sim 10^{-3}$ in the PD model). From Figure 3*b* it can be seen that the PD model with its smaller 'unit cell' than the CRN 'cell' more closely approximates the heat capacity; a unit cell containing a few hundred atoms, rather than a few thousand, would give the correct behavior at low temperatures. For comparison, a calculation with the 'supercell' of α-tridymite containing 72 atoms is shown in Figure 3*b*. This unit cell, which is the largest of the crystalline silica polymorphs, is too small to account for the excess heat capacity.

Even though the model in no way represents rigorously the physics of glass vibrations, it is strongly suggestive that the excess low-temperature heat capacity could be explained simply on the basis of low-frequency optic modes at frequencies in the spectrum where they are expected from simple structural considerations, i.e., from the general occurrence of low-frequency modes in substances which have large unit cells. A simple test of this idea would be comparison of low-temperature heat capacities of glasses of varying thermal histories (and therefore, presumably, varying structures) with high-resolution TEM micrographs. The excess heat capacity should be related to the size of any paracrystallites observed.

Rutile and Stishovite

Rutile (TiO_2) and stishovite (SiO_2) have primitive tetragonal structures with six atoms per primitive unit cell. The titanium and silicon atoms are the centers of octahedra of six oxygen atoms which occur at approximately equal distances from the cations. The unit cell of rutile (64.42×10^{-24} cm^3) is considerably larger than that of stishovite (46.54×10^{-24} cm^3) because titanium is larger than silicon. Although the geometric arrangement of the rutile structure gives little indication of anisotropy in bonding, the elastic constants are anisotropic. It has been suggested in the literature that the structure of rutile belongs to a transition type between ionic and molecular types [*Seitz*, 1940, p. 50; *Matossi*, 1951]. Thus descriptions of the vibrations in terms of modified TiO_2 molecules are not uncommon, and there might be some justification for searching for 'intramolecular' Ti-O modes of vibration, as suggested in paper 2.

From detailed measurements on anisotropic wave velocities in single-crystal rutile [*Robie and Edwards*, 1966] it is possible to obtain reasonably good estimates of the directionally averaged shear wave velocities. The velocities were calculated (appendix of paper 1) to be $u_1 = 4.73$ and $u_2 = 5.73$ km s^{-1}. Maximum and minimum shear velocities measured in high-symmetry directions are $v_{min} = 3.31$ and $v_{max} = 6.76$ km s^{-1} [*Manghnani*, 1969; *Robie and Edwards*, 1966]. The large difference between the averaged velocities u_1 and u_2 and the large difference between the minimum and maximum velocities v_{min} and v_{max}, in high-symmetry directions, both show the large degree of acoustic anisotropy characteristic of rutile. Similarly detailed measurements are not available for stishovite, and it

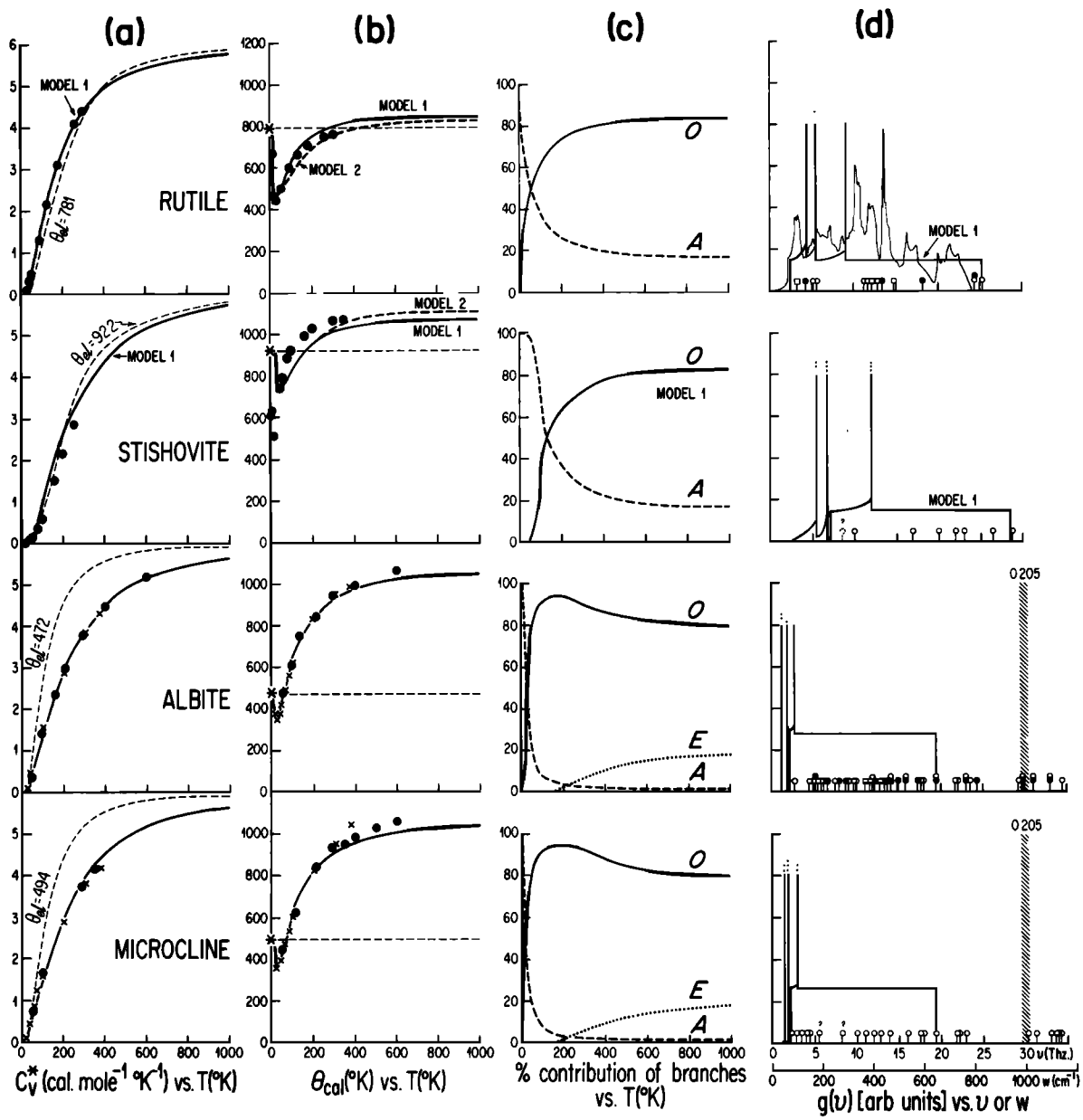

Fig. 4. Data and model values for rutile, stishovite, albite, and microcline. (*a*) Heat capacities as a function of temperature. (*b*) Calorimetric Debye temperature as a function of temperature. (*c*) Percent contribution to heat capacity of acoustic modes *A*, optic continuum *O*, and Einstein oscillator *E* as a function of temperature. (*d*) Model spectra compared to optical data or INS data. The notation is the same as that in Figure 2.

was therefore necessary to estimate the acoustic anisotropy by comparison with rutile (appendix of paper 1). The mean sound speed v_m and Debye temperature are higher for stishovite (6.16 km s^{-1} and 921°K) than for rutile (5.72 km s^{-1} and 781°K).

Acoustic branches of rutile have been measured by inelastic neutron scattering [*Traylor et al.*, 1971] (see Figure 2*e* of paper 2). Some of the branches are approximately sinusoidal (e.g., branches in the [100] direction); others deviate markedly (e.g., the longitudinal branch in the [110] direction). Anisotropy is very pronounced, for example, the difference in slopes of the longitudinal acoustic branches in the [100] and [001] is nearly a factor of 2.

The rutile INS data also show well the distribution of optic modes, their dispersion curves, and their relationship to infrared and Raman data. The lowest optical mode is at 113 cm^{-1} at **K** = 0 and is relatively flat across the Brillouin zone. This mode is one of three modes which are not active under Raman or infrared experimental conditions. Another low-frequency mode, the A_{2u}(TO) mode, is of special interest because its frequency is highly temperature dependent. The frequency of this mode drops from 172 cm^{-1} at room temperature to 140 cm^{-1} at 4°K. Although this extreme behavior may be peculiar to rutile because the *c* axis static dielectric constant is exceptionally high [*Traylor et al.*, 1971], it is not uncommon that the frequency of modes depends on temperature. Spectra obtained at room temperature and assumed to hold at low temperature may not reproduce low-temperature heat capacities because of changes in the low-frequency part of the spectrum.

The optic modes of rutile extend to 841 cm^{-1} in a fairly continuous distribution (see Figure 2 of paper 2 or Figure 4*d* of this paper). The three highest modes have been assigned as

Ti-O stretching modes [*Traylor et al.*, 1971], and it is likely that the mode at 610 cm^{-1} is a stretching mode (see discussion in paper 2). The stretching modes thus probably span the region 600–850 cm^{-1}. This is a relatively broad frequency range, and it is substantially lower than the range 1000-1200 cm^{-1} generally spanned by Si-O stretching vibrations, for which it was found that representation of the vibrations by a single Einstein oscillator at, say, 1100 cm^{-1} introduced relatively little error into C_V calculations between 0° and 1000°K. For rutile, details of the spectrum at ~700 cm^{-1} influence the heat capacity at temperatures as low as 300°K. For comparison, two models are shown: model 1 with all optic modes in the optic continuum and model 2 with one mode (0.056 of the total modes) at 610 cm^{-1} and three modes (0.167 of the total modes) at 824 cm^{-1}. The two models show appreciable differences above 200°K.

The spectrum used in the model is compared in Figure 4 with a spectrum obtained from the shell model of *Traylor et al.* [1971] by fitting of INS data. Although at low frequencies the two models agree in the representation of the optic continuum, the spectrum of this paper is significantly different from that of the Traylor model in the position of the acoustic peaks. The Traylor model does not reproduce the measured elastic Debye temperature: θ_{el} from that model is 660°K, whereas the measured value is 781°K. The model used in this paper has the correct acoustic limit, and thus the acoustic peaks are at considerably higher frequencies than those of the Traylor model.

The range of optic modes and their distribution are less well known for stishovite than for rutile because spectral data are incomplete. The lowest well-documented infrared mode is at 330 cm^{-1} (it would drop to 233 cm^{-1} at the zone boundary because of the assumed dispersion). *Striefler and Barsch* [1976] have suggested a mode at 190 cm^{-1} from rigid ion model calculations; it will be demonstrated below that such a mode would not be consistent with the measured heat capacities of stishovite. The highest infrared-active modes in stishovite are at 950 cm^{-1}. As for rutile, two models were tried: model 1 with all of the optic modes in a continuum extending to 950 cm^{-1} and model 2 with the optic continuum truncated at 769 cm^{-1} and the Si-O stretching modes as 22% of the total modes at 920 cm^{-1}.

The heat capacity for rutile is given in Figure 4*a*; the agreement with measured data is good, and the two models examined bracket the high-temperature behavior. From Figure 4*c* it can be seen that at temperatures above 50°K the heat capacity is dominated by the optic mode distribution. Rutile is unusual in that the lowest optic modes (at or near w = 113 cm^{-1}) extend below the lowest averaged shear branch (w_1 = 158 cm^{-1}). These modes cause the extreme drop in $\theta_{cal}(T)$ at low temperatures. The minimum value of $\theta_{cal}(T)$ is obtained at 25°–30°K; optic modes contribute approximately 30% of C_V at this temperature.

The two models examined for stishovite differ only in their behavior above 300°K, and because no calorimetric data exist at higher temperatures, a preferred model cannot be selected. For convenience, only model 1 (with all optic modes in the optic continuum) will be discussed further. At low temperatures the model does not match measured calorimetric data.

1. Below 40°K the model predicts a much lower heat capacity than was measured by *Holm et al.* [1967]. In this range of temperatures, only the acoustic modes contribute to C_V because the optic modes are at much too high frequency to contribute substantially. (Even Striefler and Barsch's mode at 190 cm^{-1} would not contribute to C_V below 40°K.) If this excess heat capacity were due to lattice vibrations, the vibrations would be at approximately 50 cm^{-1}, i.e., in optic modes or anomalies in the acoustic branches at about this wave number. Such modes do not appear plausible because (1) the acoustic velocities of stishovite are so high that even the extreme rutilelike anisotropy assumed does not give a low-frequency shear branch anomaly at 50 cm^{-1}; (2) dispersion does not generally play a role until $w \sim 0.5w_1$, i.e., to about 80 cm^{-1} in this case; and (3) optic modes do not generally lie below the lowest shear branch which, in the case of stishovite, is at 158 cm^{-1} at the Brillouin zone boundary. However, if the low-frequency modes observed in rutile were characteristic of minerals with the rutile structure, a low-frequency optic mode below w_1 would be possible. Simple cation mass scaling from the frequency of the lowest rutile mode would suggest that this mode would be near $w_{l,\text{rutile}} \times (m_{Ti}/m_{Si})^{1/2} \approx 150$ cm^{-1}, far above the wave number of 50 cm^{-1} required to explain the excess heat capacity. It therefore seems unlikely that the drop of the measured $\theta_{cal}(T)$ to the low minimum is explicable by anisotropy, dispersion, or low-frequency optic modes. Another cause for this anomaly was suggested by *Holm et al.* [1967], who obtained the calorimetric data: that the excess heat capacity arises from surface contributions because the mean particle size in the heat capacity experiments was 740 Å [*Holm et al.*, 1967]. To the extent that these model calculations do not match the low-temperature C_V data when reasonable lattice behavior is assumed, the model considerations suggest that the excess heat capacity could be from nonlattice effects such as surface energy. The model may therefore give an appreciably better estimate of the lattice heat capacity below 50°K than the data.

2. Above 40°K the model overestimates the heat capacity in comparison to calorimetric data. Because optic modes dominate in this temperature range, the behavior must be due to an excess of optic modes at frequencies between 200 and 300 cm^{-1}; i.e., it is probably due to a poor estimate of the lower cutoff frequency of the optic continuum. Use of the *Striefler and Barsch* [1976] value of 190 cm^{-1} for w_l would only increase the discrepancy between the model values and the calorimetric value.

In the case of stishovite there are uncertainties in all of the data examined: acoustic velocities, spectral data, and calorimetric data. Therefore each data set should be subjected to reexamination. Nevertheless, the model proposed gives an estimate of the heat capacity which is probably more realistic than the Debye model, gives some insight into the vibrational spectrum, and affords more detailed comparison with the properties of rutile than does the Debye model.

Albite and Microcline

Albite ($NaAlSi_3O_8$) and microcline ($KAlSi_3O_8$) contain 52 atoms in their monoclinic unit cells. The state of Al-Si disorder affects the thermodynamic properties but is not considered here because detailed descriptions of the samples used for the acoustic and optical parameters are not available. An excellent discussion of the effect of the ordering parameter on thermodynamic properties is given by *Openshaw* [1974]. For all practical purposes this paper assumes completely ordered albite and microcline.

Because there are 156 degrees of freedom in the unit cell, the three acoustic branches account for only 2% of the total vibrational modes. The acoustic velocities of the feldspars are among the lowest measured for minerals. The difference in velocities between albite and microcline is insignificant in the model. Because of the low acoustic velocities and large unit cell (small Brillouin zone) the acoustic branches are limited to

very low wave numbers: 45, 60, and 92 cm^{-1} for w_1, w_2, and w_3 in albite and 45, 47, and 89 cm^{-1} in microcline.

As might be expected from these low values for the acoustic peaks and from the discussion in paper 2, optic modes occur at very low frequencies. A weak infrared mode occurs at 83 cm^{-1} in albite; a well-documented infrared mode occurs at 98 cm^{-1} in microcline, and *Iiishi et al.* [1971] suggested an even lower mode at 74 cm^{-1}. This lower mode was used in the model because although it was not documented in the Kieffer observations (see Figure 1 of paper 2), the discussion below suggests that it may be a Raman-active mode observed for some reason by Iiishi et al. in the infrared experiment. These low modes are associated with K-O or Na-O cation-oxygen vibrations [*Iiishi et al.*, 1971]. The modes are lowered by the assumed dispersion to 63 and 62 cm^{-1} for albite and microcline, respectively. Optic modes arising from Si(Al)-O bending, deformation, and torsion extend out to ~800 cm^{-1} [*Iiishi et al.*, 1971, p. 108]. These modes are represented by the optic continuum in the model. The 20.5% of the modes attributed to Si(Al)-O stretching (in paper 2) cover a broad band from 720 to 1050 cm^{-1} in both minerals. They are represented by a single Einstein oscillator at 1000 cm^{-1} in this paper.

The heat capacities predicted by the model are shown in Figure 4*a*, where they are compared with measured data. For albite, optic modes contribute half of the heat capacity by 20°K; by this temperature, the heat capacity has nearly risen back to the value of the elastic Debye temperature, 471°K. The subsequent rise of $\theta_{cal}(T)$ between 30°K and 400°–500°K is caused by the spread of bending and deformation modes over a wide range of frequencies. The model heat capacity is slightly too large at high temperatures, but on the whole the representation is much better than a Debye model. (It might be of interest to the reader that when the lowest IR band of albite at 92 cm^{-1} was initially used in the model, the heat capacity at 20°–50°K was not accurately reproduced. This led me to hypothesize that the slight shoulder at 83 cm^{-1} on the IR spectrum (Figure 1*d* of paper 2) was a Raman-active, IR-forbidden line. J. Delany subsequently obtained a Raman spectrum on albite and found the 83-cm^{-1} band. Although the real strength of the model lies in using spectral data to calculate the calorimetric functions, I believe that this capability of using the calorimetric data to infer limits on the spectra illustrates the very strong relationship between the spectroscopic and the thermodynamic data.)

The importance of the low-frequency optic vibrations must be reemphasized here. The distribution of these optic vibrations, which arise from cation-oxygen motions, dominates the heat capacity behavior in the range 30°–100°K. This is precisely the range of temperatures which contributes most heavily to the entropy. Therefore an accurate estimate of the entropy, say, S_{298}^0, cannot be made from acoustic wave velocities but only from a reasonably complete knowledge of the low-frequency optic mode distribution.

6. SUMMARY

A form for a simplified vibrational spectrum generally applicable to minerals has been proposed and applied to a number of simple minerals and framework silicates in this paper. The purpose was to examine systematic relationships between structure, composition, and the thermodynamic functions. The temperature dependence of the heat capacity was examined here and will be given in paper 4 for chain, sheet, and orthosilicates; pressure and temperature dependences of heat capacity, entropy, enthalpy, and Helmholtz free energy will be given in paper 5 of this series.

The fundamental assumption underlying the theory developed here is that the basic vibrating unit of a crystal is the primitive unit cell. From this assumption, which is rooted in Bloch's theorem of translational periodicity, it follows that acoustic modes comprise 3 out of 3*s* degrees of freedom, where *s* is the number of atoms in a unit cell. Because minerals generally have large unit cells with many atoms, the acoustic modes are generally a minor fraction of the total modes. Therefore acoustic data alone reveal little about the thermodynamic properties of complex substances except at temperatures of a few degrees Kelvin.

The model spectra are only approximations to real spectra but are correct in their enumeration of the fraction of the modes which are acoustic and in representation of the actual regions of frequency in which there are vibrational modes. The spectra provide good estimates of the heat capacity because the thermodynamic functions are averages over the whole frequency distribution and are insensitive to details of the spectrum (except at low temperature). An approximating spectrum such as the one proposed, valid for a wide variety of minerals, is a useful tool for correlating thermodynamic properties with elastic properties, optical spectra, and inelastic neutron scattering data.

Structure and composition of minerals influence the thermodynamic properties in the following ways.

1. The density of the mineral is generally directly related (a monotonically increasing function) to the acoustic velocities and therefore to the slopes of the acoustic branches.
2. The volume of the unit cell determines the size of the Brillouin zone and thus the proportion and extent of the acoustic branches. Large unit cells have small Brillouin zones and therefore low-frequency cutoffs for the acoustic branches.
3. The number of atoms in a unit cell determines the total number of degrees of freedom and thus the fractions which are in acoustic and optic modes.
4. Atomic masses and force constants determine the absolute values of lattice vibrational frequencies; atomic mass and force constant ratios determine the 'stopping band' between acoustic and optic modes.
5. Tightly bound clusters within silicates may contain an appreciable fraction of the total modes at isolated frequencies. The fraction of vibrations associated with intramolecular stretching modes is easily calculable from simple analysis of the structure.

The investigation of the mineral heat capacities in terms of the model has revealed the following general sensitivities of the heat capacities to spectral details:

1. The specific heat below about 50°K cannot be reproduced accurately unless spectral details below 150 cm^{-1} are known to a resolution of about 10 cm^{-1}; hence model accuracy may be limited to ±50% because neither acoustic nor optic spectral data are known with sufficient precision in this range of wave numbers.
2. The specific heat above 50°K can be predicted reasonably well if the general range spanned by optic modes is known. The model accuracy is typically ±5% at 298°K for minerals for which IR spectra are available.
3. The specific heat at high temperature, above 300°K, is relatively insensitive to details of the high-frequency part of the spectrum. In particular, it is generally adequate to model

the Si-O stretching modes, which may cover a range of 300 cm^{-1}, by a single Einstein oscillator at a mean frequency. The model typically has an accuracy of ±1% at 700°K.

Applicability of the model to a large number of minerals and accuracy for those to which it is applied is limited by the paucity of data at wave numbers below 200 cm^{-1} and the sensitivity of the thermodynamic properties to the details of the vibrational spectrum at low frequencies. The lower cutoff frequency of the optic continuum has probably rarely been observed in optical spectra for two reasons: (1) there is a general lack of low-frequency optical data on minerals; such data, at $\mathbf{K} = \mathbf{0}$, would provide an estimate of w_l; and (2) from theoretical considerations the lowest values of w_l are expected at $\mathbf{K} = \mathbf{K}_{max}$ rather than at $\mathbf{K} = \mathbf{0}$ (see Figure 7 of paper 1 and Figure 2 of paper 2). Therefore the accuracy to which low-temperature thermodynamic properties (which depend heavily on the value of w_l) can be predicted is limited if INS data are not available and only data at $\mathbf{K} = \mathbf{0}$ are available.

The model is useful in the form presented here as a method of predicting thermodynamic properties of minerals; the method is independent of any calorimetric data. Because of nonharmonic contributions to the thermodynamic properties not accounted for in the model, the calculations cannot replace calorimetric determinations, but will be primarily useful in (1) providing good estimates of the thermodynamic properties of materials for which there are insufficient samples, for samples which are of poor quality for calorimetric work, or for materials which are unstable, e.g., stishovite, and (2) providing a framework to interrelate thermodynamic, spectroscopic, acoustic, and structural data.

NOTATION

Equation numbers given refer to the first use of the symbol in an equation or to the equations nearest the first occurrence of the symbol in the text.

$\mathbf{a}_1, \mathbf{a}_2, \mathbf{a}_3$ basic vectors of the primitive lattice, before (1).
A coefficient for low-temperature C_V of glass, (32) only.
B bulk modulus, (29).
B coefficient for low-temperature C_V of glass, (32) only.
c speed of light.
$C_{\alpha\beta}$ lattice potential coefficients, (5).
C_P heat capacity (molar) at constant pressure, (29).
C_V heat capacity (molar) at constant volume (7).
C_V^E heat capacity (molar) of an Einstein oscillator (same as $\mathcal{E}(\hbar\omega/kT)$ in paper 1 and as $\mathcal{E}(x_E)$), (24).
C_V^* heat capacity (molar) normalized to monatomic equivalent, (21).
E^* internal energy (molar) normalized to monatomic equivalent, (26).
$\mathcal{E}(x_E)$ Einstein function, (7) and (24).
F^* Helmholtz free energy (molar) normalized to monatomic equivalent, (28).
$g(\mathbf{K}), g(\omega)$ frequency distribution function, between (6) and (7).
$g_i(\mathbf{K}), g_i(\omega)$ frequency distribution of acoustic branch i, where $i = 1, 2, 3$, (12a).
g_0 frequency distribution of optical continuum, (19).
g_E frequency distribution for an Einstein oscillator, (18).
h Planck constant, equal to 6.625×10^{-27} ergs s.
$\hbar$ Planck constant divided by 2π.
j, j' cell index, before (1).
k Boltzmann constant, equal to 1.380×10^{-16} ergs deg^{-1}.
$\mathbf{K}(\eta)$ wave vector, before (1) ((2) in paper 1).
$\mathbf{K}_{max}$ maximum wave vector (Brillouin zone boundary), (8).
$\mathcal{K}\left(\begin{smallmatrix} x_u \\ x_l \end{smallmatrix}\right)$ optic continuum function, (23).
m_r particle mass, (1).
N_A Avogadro's number, equal to 6.023×10^{23} mol^{-1}, before (1).
n number of atoms in the chemical formula on which the molar volume is defined, before (1).
q proportion of vibrational modes in Einstein oscillator, (18).
R gas constant per mole, equal to 1.988 cal mol^{-1} deg^{-1}), (21).
r, r' base index, before (1).
s number of particles in Bravais unit cell, before (1).
S^* entropy (molar) normalized to monatomic equivalent, (27).
$\mathcal{S}(x_l)$ dispersed acoustic function, (22).
T temperature, degrees Kelvin unless otherwise indicated, (7).
u_l spatially averaged acoustic velocity for acoustic branches i, where $i = 1, 2, 3$, before (10).
$v(\theta, \phi)$ acoustic velocity, (10).
V molar volume, (8).
V_L volume of unit cell, (8).
V_R volume of unit cell of reciprocal lattice (Brillouin zone), (8).
w wave number, equal to $\omega/2\pi c$ cm^{-1}, between (25) and (26).
w_1, w_2, w_3 wave numbers of acoustic branches at Brillouin zone boundary, where $i = 1, 2$ for shear branches and $i = 3$ for longitudinal branch.
$W_\alpha(r)$ wave amplitude, (4).
$\mathbf{x}(j)$ general position vector, before (1).
$\mathbf{x}(j)$ distance of unit cell from origin, before (1).
$\mathbf{x}(r)$ position of a particle within a unit cell, before (1).
x dimensionless frequency ($\hbar\omega/kT$), (22).
$\mathbf{y}$ reciprocal lattice vector, equal to $\mathbf{K}/2$, after (4).
Z number of 'molecules' in Bravais unit cell, before (1).
α' summation index, (1)–(6) only.
β' summation index, (2)–(6) only.
γ thermal Grüneisen parameter, (31).
$\delta_{\alpha'\beta'}$ Kronecker delta function, (6).
$\delta(\omega - \omega_E)$ Dirac delta function, (18).
ϵ thermal expansion, (29).
$\theta_{cal}(T)$ calorimetric Debye temperature, after (6).
θ_D Debye temperature, after (31).
θ_{el} elastic Debye temperature, after (31).
(θ, ϕ) direction angles, (10).
λ_{min} cutoff wavelength, (9).
$\mu(j), \mu_\alpha(j)$ displacement of a point at $\mathbf{x}$ in the crystal; components $\mu_\alpha(j)$, $\alpha = 1, 2, 3$, (1).

ν frequency, cycles per second or terahertz, between (4) and (5).

ρ_0, ρ_T density at 0°K and at temperature T, (31).

Φ potential energy of the lattice, (1).

ω angular frequency, radians per second, (4).

ω_E Einstein frequency, (18).

$\omega_i(K)$ Frequency of branch i, where $i = 1, 2, \cdots, 3s$, after (6); from section 3 to end of paper, refers to acoustic branches, $i = 1, 2, 3$.

$\omega_{i,\max}$ maximum frequency of acoustic branch i, $i = 1, 2, 3$, (11); after (17) shortened to ω_i.

ω_l lower frequency limit of optical continuum, (19).

ω_u upper frequency limit of optical continuum, (19).

Ω solid angle, (10).

Acknowledgments. In the early days of this work (nearly 10 years ago), Barclay Kamb gave generously of his time, not as one man, but as all six of Kipling's honest serving men: his name was 'What and Why and When, and How and Where and Who.' I gratefully acknowledge those many fun hours of relentless questioning and spirited discussion. This work was begun as a Ph.D. dissertation at the California Institute of Technology (CIT); the manuscripts were completed while the author was an Alfred P. Sloan Research Fellow at UCLA. I thank the Sloan Foundation for support which allowed the time and freedom for culmination of the project. The efforts of Art Boettcher as Associate Editor in securing many reviews of this paper and the helpful and thought-provoking comments and questions by Roger Burns and other reviewers were greatly appreciated, although the author bears sole responsibility for errors which may remain. Barbara Niles (CIT), B. Gola, Gen Kurtin, Barbara Nielsen, and Vicki Doyle-Jones (UCLA) contributed extraordinary efforts in typing and drafting the many manuscripts. Funds for computer calculations were provided initially by intramural funding at the California Institute of Technology and then at the University of California at Los Angeles.

REFERENCES

Anderson, O. L., The Debye temperature of vitreous silica, *Phys. Chem. Solids, 12,* 41–52, 1959.

Anderson, O. L., and H. E. Bömmel, Ultrasonic absorption in fused silica at low temperatures and high frequencies, *J. Amer. Ceram. Soc., 38,* 125–131, 1955.

Anderson, O. L., and R. C. Liebermann, Sound velocities in rocks and minerals, *Contract Rep. 7885-4-X,* 182 pp., Willow Run Lab., Ann Arbor, Mich., 1966.

Antoniou, A. A., and J. A. Morrison, Low-temperature heat capacity of vitreous germania, *J. Appl. Phys., 36*(6), 1873–1877, 1965.

Barron, T. H. K., and R. W. Munn, Heat capacities of non-cubic solids, *Proc. Phys. Soc. London, Sect. C, 2,* 1–10, 1968.

Barron, T. H. K., W. T. Berg, and J. A. Morrison, On the heat capacity of crystalline magnesium oxide, *Proc. Roy. Soc. London, Ser. A., 250,* 70–83, 1959.

Bell, R. J., and P. Dean, Properties of vitreous silica: Analysis of random network models, *Nature London, 212,* 1354–1356, 1966.

Bell, R. J., and P. Dean, Atomic vibrations in vitreous silica, *Discuss. Faraday Soc., 50,* 55–61, 1970.

Bell, R. J., N. F. Bird, and P. Dean, The vibrational spectra of vitreous silica germania and beryllium fluoride, *J. Phys. C., 1,* 299–303, 1968.

Blackman, M., The specific heat of solids, in *Handbuch der Physik,* vol. 7, part 1, pp. 325–382, Springer, New York, 1955.

Born, M., and K. Huang, *Dynamical Theory of Crystal Lattices,* 420 pp., Oxford University Press, New York, 1954.

Bragg, L., G. F. Claringbull, and L. H. Taylor, *Crystal Structure of Minerals,* 409 pp., Cornell University Press, New York, 1965.

Brillouin, L., *Wave Propagation in Periodic Structures,* 255 pp., Dover, New York, 1953.

Clark, A. E., and R. E. Strakna, The low temperature excess specific heat of SiO_2 glass, *Phys. Chem. Glasses, 3*(4), 121–126, 1962.

Clark, S. P., *Handbook of Physical Constants, Mem. 97,* Geological Society of America, Boulder, Colo., 1966.

Cochran, W., Lattice dynamics of ionic and covalent crystals, *Crit. Rev. Solid State Sci., 2*(1), 1–44, 1971.

De Sorbo, W., The effect of lattice anisotropy on low-temperature specific heat, *Acta Met., 2,* 274–283, 1954.

Dixon, A. E., A. D. B. Woods, and B. N. Brockhouse, Frequency distribution of the lattice vibrations in sodium, *Proc. Phys. Soc. London, 81,* 973–974, 1963.

Elcombe, M. H., Some aspects of the lattice dynamics of quartz, *Proc. Phys. Soc. London, 91,* 947–958, 1967.

Evans, D. L., and S. V. King, Random network model of vitreous silica, *Nature London, 212,* 1353–1354, 1966.

Flubacher, P., A. J. Leadbetter, J. A. Morrison, and B. P. Stoicheff, The low-temperature heat capacity and the Raman and Brillouin spectra of vitreous silica, *J. Phys. Chem. Solids, 12,* 53–65, 1959.

Fraas, L. M., and J. E. Moore, Raman selection rule violation for a spinel crystal, *Rev. Brasil. Fis., 2*(3), 299–310, 1972.

Freund, F., and V. Sperling, Hydrogen bonding in $Mg(OH)_2$ and its effect on specific heat and thermal expansion, in *Thermal Analyses Proceedings Third ICTA, Davos, Switzerland,* edited by H. G. Wiedemann, vol. 2, pp. 381–392, Birkhauser, Basel, Switzerland, 1972.

Fritzsche, H., A review of some electronic properties of amorphous substances, in *Electron and Structural Properties of Amorphous Semiconductors,* edited by P. G. Le Comber and J. Mort, pp. 55–123, Academic, New York, 1973.

Gaskell, P. H., Vibrational spectra of simple silicate glasses, *Discuss. Faraday Soc., 50,* 82–93, 1970.

Gaskell, P. H., and A. Howie, High resolution electron microscopy of amorphous semiconductors and oxide glasses, in *Proceedings of the 12th International Conference on Physics of Semiconductors, July 15–19, 1974,* edited by M. H. Pilkuhn, pp. 1076–1080, Truebner, Stuttgart, West Germany, 1974.

Giauque, W. F., and R. C. Archibald, The entropy of water from the third law of thermodynamics: The dissociation pressure and calorimetric heat of the reaction $Mg(OH)_2 = MgO = H_2O$: The heat capacities of $Mg(OH)_2$ and MgO from 20 to 300°K, *J. Amer. Chem. Soc., 59,* 561–569, 1937.

Gopal, E. S. R., *Specific Heats at Low Temperatures,* Plenum, New York, 1966.

Holm, J. L., O. L. Kleppa, and E. F. Westrum, Jr., Thermodynamics of polymorphic transformations in silica: Thermal properties from 5 to 1070°K and pressure-temperature stability fields for coesite and stishovite, *Geochim. Cosmochim. Acta, 31,* 2289–2307, 1967.

Iiishi, K., T. Tomisaka, T. Kato, and Y. Umegaki, Isomorphous substitution and infrared and far infrared spectra of the feldspar group, *Neues Jahrb. Mineral. Abh., 115,* 98–119, 1971.

Janaff, Thermochemical tables, Joint Army, Navy, and Air Force Project Principia of the Advanced Research Projects Agency, *Rep. PB 168 370,* Therm. Res. Lab., Dow Chem. Co., Midland, Mich., 1965*a*. (Also available from Clearinghouse, U.S. Dep. of Commer., Springfield, Va.)

Janaff, Thermochemical tables, first addendum, Joint Army, Navy, and Air Force Project Principia of the Advanced Research Projects Agency, Therm. Res. Lab., Dow Chem. Co., Midland, Mich., 1965*b*.

Janaff, Thermochemical tables, second addendum, Joint Army, Navy, and Air Force Project Principia of the Advanced Research Projects Agency, Therm. Res. Lab., Dow Chem. Co., Midland, Mich., 1966.

Janaff, Thermochemical tables, third addendum, Joint Army, Navy, and Air Force Project Principia of the Advanced Research Projects Agency, Therm. Res. Lab., Dow Chem. Co., Midland, Mich., 1967.

Kam, Z., and G. Gilat, Accurate numerical method for calculating frequency distribution functions in solids, III, Extension to tetragonal crystals, *Phys. Rev., 175,* 1156–1163, 1968.

Kellerman, E. W., On the specific heat of the sodium chloride crystal, *Proc. Roy. Soc. London, Ser. A, 178,* 17–24, 1940.

Kelley, K. K., Heat capacities of ethyl and hexyl alcohols from 16°K to 298°K and the corresponding entropies and free energies, *J. Amer. Chem. Soc., 51,* 779–786, 1929.

Kelley, K. K., S. S. Todd, R. L. Orr, E. G. King, and K. R. Bonnickson, Thermal properties of sodium-aluminum and potassium-aluminum silicates, *U.S. Bur. Mines Rep. Invest., 4955,* 1953.

Kieffer, S. W., Thermodynamics and lattice vibrations of minerals, 1, Mineral heat capacities and their relationships to simple lattice

vibrational models, *Rev. Geophys. Space Phys., 17,* this issue, 1979*a*.
Kieffer, S. W., Thermodynamics and lattice vibrations of minerals, 2, Vibrational characteristics of silicates, *Rev. Geophys. Space Phys., 17,* this issue, 1979*b*.
Leadbetter, A. J., Inelastic cold neutron scattering from different forms of silica, *J. Chem. Phys., 51,* 779–786, 1969.
Leadbetter, A. J., and D. Litchinsky, Vibrational properties of vitreous germania by inelastic cold neutron scatterning, *Discuss. Faraday Soc., 50,* 62–73, 1970.
Leibfried, G., Gittertheorie der mechanischen und thermischen Ergenschaften der Kristalle, in *Handbuch der Physik,* vol. 7, part 1, pp. 104–324, Springer, New York, 1955.
Leibfried, G., and W. Ludwig, Theory of anharmonic effects in crystals, *Solid State Phys., 12,* suppl., 275–444, 1961.
Lord, R. C., and J. C. Morrow, Calculation of the heat capacity of α-quartz and vitreous silica from spectroscopic data, *J. Chem. Phys., 26,* 230–232, 1957.
Manghnani, M., Elastic constants of single-crystal rutile under pressures to 7.5 kbar, *J. Geophys. Res., 74,* 4317–4328, 1969.
Maradudin, A. A., E. W. Montroll, and G. H. Weiss, *Lattice Dynamics in the Harmonic Approximation,* 319 pp., Academic, New York, 1963.
Matossi, F., The vibration spectrum of rutile, *J. Chem. Phys., 19,* 1543–1546, 1951.
McSkimmin, H. J., P. Andreatch, Jr., and R. N. Thurston, Elastic moduli of quartz versus hydrostatic pressure at 25° and −195.8°C, *J. Appl. Phys., 36,* 1624–1632, 1965.
Mizutani, H., Y. Hamano, and S. Akimoto, Elastic wave velocities of polycrystalline stishovite, *J. Geophys. Res., 77,* 3744–3749, 1972.
Montroll, E. W., Frequency spectrum of crystalline solids, *J. Chem. Phys., 10,* 218–229, 1942.
Montroll, E. W., Frequency spectrum of crystalline solids, II, General theory and applications to simple cubic lattices, *J. Chem. Phys., 11,* 481–495, 1943.
Neuberger, J., and R. D. Hatcher, Infrared optical constants of NaCl, *J. Chem. Phys., 34,* 1733, 1961.
Newell, G. F., Specific heat of lamellar crystals, *J. Chem. Phys., 23,* 2431–2438, 1955.
Openshaw, R., The low temperature heat capacities of annalbite, low albite, microcline, and sanidine, Ph.D. thesis, 312 pp., Princeton Univ., Princeton, N. J., 1974.
Pelah, I., K. Krebs, and Y. Imry, Inelastic neutron spectra and the vibrational modes of the hydrogen layer in alkali and alkaline-earth hydroxides, *J. Chem. Phys., 43*(6), 1864–1869, 1965.
Prebus, A. F., and J. W. Michener, Electron microscope observations of glass, *Ind. Eng. Chem., 46*(1), 147–153, 1954.
Preudhomme, J., and P. Tarte, Infrared spectra of spinels, I, A critical discussion of the actual interpretation, *Spectrochim. Acta, Part A, 27,* 961–968, 1971*a*.
Preudhomme, J., and P. Tarte, Infrared spectra of spinels, II, The experiment bases for solving the assignment problem, *Spectrochim. Acta, Part A, 27,* 845–851, 1971*b*.
Preudhomme, J., and P. Tarte, Infrared spectra of spinels, III, The normal II-III spinels, *Spectrochim, Acta, Part A, 27,* 1817–1835, 1971*c*.
Preudhomme, J., and P. Tarte, Infrared studies of spinels, IV, Normal spinels with a high valency cation, *Spectrochim. Acta, Part A, 28,* 1972.
Raman, C. V., The vibration spectrum of a crystal lattice, *Proc. Indian Acad. Sci., 18,* 237–250, 1943.
Raman, C. V., The vibrations of the MgO crystal structure and its infrared absorption spectrum, *Proc. Indian Acad. Sci., 54,* 202–252, 1961.
Randall, J. T., H. P. Rooksby, and B. S. Cooper, X-ray diffraction and the structure of vitreous solids, *Z. Kristallogr. Kristallgeometrie Kristallphys. Krystallchem., 75,* 196–214, 1930.
Raubenheimer, L. J., and G. Gilat, Accurate numerical method of calculating frequency distribution functions in solids, II, Extension to hcp crystals, *Phys. Rev., 157,* 586–599, 1967.
Raunio, G., L. Almqvist, and R. Stedman, Phonon dispersion relations in NaCl, *Phys. Rev., 178,* 1496–1501, 1969.
Robie, R. A., and J. L. Edwards, Some Debye temperatures from single-crystal elastic constant data, *J. Appl. Phys., 37,* 2659–2663, 1966.
Robie, R. A., B. S. Hemingway, and W. H. Wilson, Low-temperature heat capacities and entropies of feldspar glasses and of anorthite, *Amer. Mineral., 63,* 109–123, 1978.
Robinson, H. A., On the structure of vitreous SiO_2, I, A new pentagonal dodecahedral model, *J. Phys. Chem. Solids, 26,* 209–222, 1965.
Safford, G., V. Brajovic, and H. Boutin, An investigation of the energy levels in alkaline earth hydroxides by inelastic scattering of slow neutrons, *Phys. Chem. solids, 24,* 771–777, 1963.
Saksena, B. D., Infra-red absorption studies of some silicate structures, *Trans. Faraday Soc., 57,* 242–258, 1961.
Seitz, F., *The Modern Theory of Solids,* 698 pp., McGraw Hill, New York, 1940.
Simakov, G. V., M. N. Pavlovskiy, N. G. Kalashnikov, and R. F. Trunin, Shock compressiblity of twelve minerals, *Izv. Acad. Sci. USSR Phys. Solid Earth,* Engl. Transl., *8,* 11–17, 1974.
Smythe, H. T., H. S. Skogen, and W. B. Harsell, Thermal capacity of vitreous silica, *J. Amer. Ceram. Soc., 36,* 327–328, 1953.
Sosman, R. B., *The Phases of Silica,* 388 pp., Rutgers University Press, New Brunswick, N. J., 1965.
Striefler, M. E., and G. R. Barsch, Elastic and optical properties of stishovite, *J. Geophys. Res., 81*(14), 2453–2466, 1976.
Tarasov, V. V., Theory of the heat capacity of chain and layer structures (in Russian), *Zh. Fiz. Khim., 24,* 111–128, 1950.
Traylor, J. G., H. G. Smith, R. M. Nicklow, and M. K. Wilkinson, Lattice dynamics of rutile, *Phys. Rev. B, 3*(10), 3457–3472, 1971.
Valenkov, N., and E. Porai-Koshitz, X-ray investigation of the glassy state, *Z. Kristallogr. Kristallgeometrie Kristallphys. Kristallchem., 95,* 195–229, 1936.
Walker, C. B., X-ray study of lattice vibrations in aluminum, *Phys. Rev., 103,* 547–557, 1956.
Wallace, D. C., *Thermodynamics of Crystals,* 484 pp., John Wiley, New York, 1972.
Warren, B. E., X-ray diffraction of vitreous silica, *Z. Kristallogr. Kristallgeometrie Kristallphys. Kristallchem., 86,* 349, 1933.
Warren, B. E., X-ray determination of structure of glass, *J. Amer. Ceram. Soc., 17,* 249–254, 1934.
Warren, B. E., Determination of structure of liquids and glass, *J. Appl. Phys., 8,* 645–654, 1937.
Warren, B. E., and J. J. Biscoe, The structure of silica glass by x-ray diffraction studies, *J. Amer. Chem. Soc., 21,* 49–59, 1938.
Wong, P. T. T., and E. Whalley, Infrared and Raman spectra of glasses, *Discuss. Faraday Soc., 50,* 94–103, 1970.
Zacharaisen, W. H., The atomic arrangement in glass, *J. Amer. Chem. Soc., 54,* 3841–3851, 1932.
Zacharaisen, W. H., The vitreous state, comments on the article by Gunnar Hagg, the vitreous state, *J. Chem. Phys., 3,* 162–163, 1935.
Zarzychi, J., and R. Mezard, A direct electron microscope study of the structure of glass, *Phys. Chem. Glasses, 3*(5), 163–166, 1962.
Zeller, R. C., and R. O. Pohl, Thermal conductivity and specific heat of noncrystalline solids, *Phys. Rev. B., 4,* 2029–2041, 1971.
Ziman, J. M., *Principles of the Theory of Solids,* 435 pp., Cambridge, University Press, New York, 1972.

(Received May 24, 1978;
accepted September 22, 1978.)